nature protocols

PROTOCOL

https://doi.org/10.1038/s41596-019-0174-2

Solvent-assisted preparation of supported lipid bilayers

Abdul Rahim Ferhan[1], Bo Kyeong Yoon[1], Soohyun Park[1], Tun Naw Sut[1], Hokyun Chin[1], Jae Hyeon Park[1], Joshua A. Jackman[2*] and Nam-Joon Cho[1,3*]

The supported lipid bilayer (SLB) platform is a popular cell membrane mimic that is utilized in the chemical, biological, materials science, and medical fields. To date, SLB preparation has proven challenging because of the need for specialized fabrication equipment, domain-specific knowledge about topics relevant to lipid self-assembly, and extensive training in the interfacial science field. Existing methods, such as vesicle fusion, also work with only a narrow range of lipid compositions and material supports. Here, we describe a recently developed simple and versatile protocol to form SLBs. The protocol is simple because it requires minimal sample preparation and only basic microfluidics, making it technically accessible to researchers across different scientific disciplines. The protocol is versatile because it works on a wide range of material supports, such as silicon oxide, gold, and graphene, and is compatible with diverse lipid compositions, including sterols and signaling lipids. The main stages of the procedure involve dissolving a lipid sample in an organic solvent, depositing the lipid solution on a solid support, and replacing the organic solvent with aqueous buffer. In addition, we provide procedures for characterizing the quality of the prepared SLBs and present examples of biofunctionalization procedures. The protocol takes 1–2 h and is broadly useful in various application contexts, including clinical diagnostics, biosensing, and cellular interfaces.

Introduction

SLBs are 2D lipid bilayer films that mimic key architectural features of cellular membranes and can be fabricated on solid supports[1–3]. Since their invention several decades ago, SLBs have been widely studied in order to understand the structure and function of lipid bilayer assemblies, to investigate biomacromolecular interactions, and to develop lipid membrane technologies for various application areas[4–7]. In addition to broad application possibilities, one of the most compelling features of SLBs is that they are compatible with a wide range of surface-sensitive measurement techniques[8–13]. Such tools have enabled deep understanding of the mechanisms associated with SLB formation and corresponding biological processes (e.g., membrane fusion), as well as provided insights helpful in devising improved fabrication strategies aimed at (i) increasing SLB formation efficiency, (ii) expanding the range of material supports on which SLBs can be formed, (iii) designing more biologically relevant SLBs with diverse compositions, and (iv) improving the ease of SLB fabrication procedures so that they can be adopted by researchers from different scientific disciplines.

In this protocol, we present detailed procedures for the formation of SLBs on solid supports by using the solvent-assisted lipid bilayer (SALB) method[14], which is a recently developed approach that overcomes the challenges of existing methods while greatly expanding the scope of fabrication possibilities. The SALB method is innovative because it requires minimal sample preparation, namely dissolving lipids in a suitable organic solvent. The process is quick and efficient, comprising deposition of the lipid solution on a solid support, followed by exchange of the organic solvent with an aqueous buffer. Although simple, the SALB method also overcomes one of the biggest challenges in SLB fabrication: it provides a truly bottom-up fabrication process that does not require specialized equipment or technical expertise. As such, well-developed protocols that utilize the SALB method provide a simple and versatile option for SLB preparation and can be widely adopted by researchers from different scientific fields. With recent reporting of detailed procedures to prepare solution-phase

[1]School of Materials Science and Engineering, Nanyang Technological University, Singapore, Singapore. [2]School of Chemical Engineering, Sungkyunkwan University, Suwon, Republic of Korea. [3]School of Chemical and Biomedical Engineering, Nanyang Technological University, Singapore, Singapore. *e-mail: jjackman@skku.edu; njcho@ntu.edu.sg

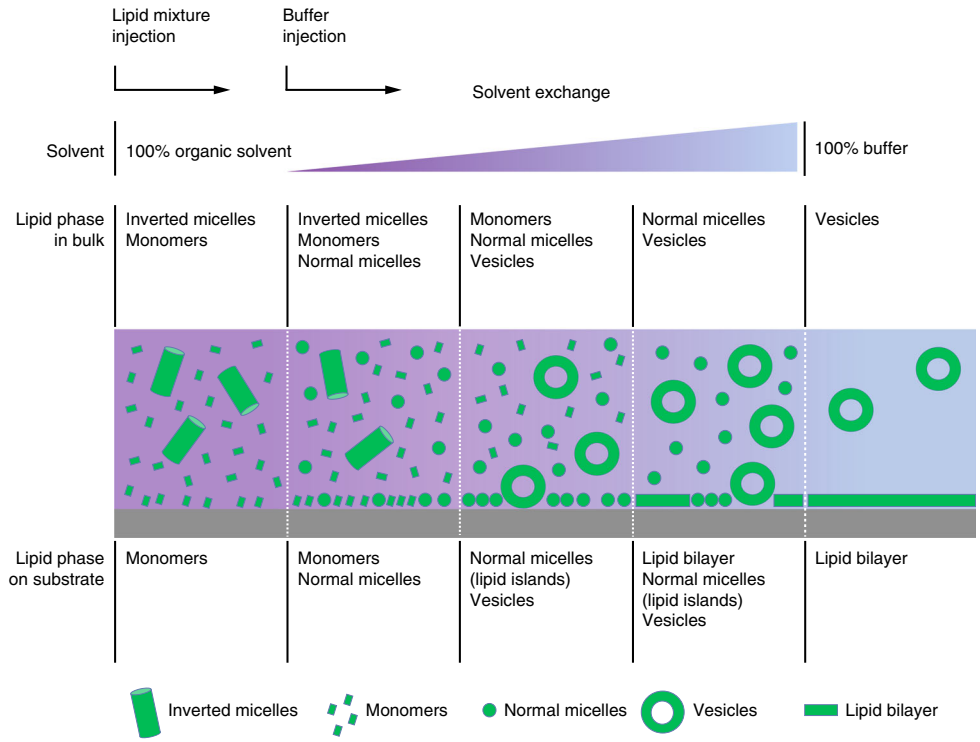

Fig. 1 | Molecular self-assembly of phospholipid molecules in different solvent systems. In organic solvent, phospholipid molecules often assemble into inverted micelles or remain as monomers. With increasing water fraction in the solvent system, phospholipid molecules tend to assemble into normal micelles or vesicles. By adjusting the solvent environment during the course of an experiment, it is possible to utilize these self-assembly principles to promote SLB formation on a solid support.

liposomes[15,16], our protocol provides a complementary approach to aid researchers interested in preparing cell membrane–mimicking platforms on solid supports.

Development of the protocol

The molecular self-assembly of phospholipids depends on the solvent environment, with different supramolecular structures forming in aqueous and organic solvents. Early work demonstrated the generation of large unilamellar vesicles in a bulk solution, whereby aqueous buffer is introduced into a mixture of phospholipids and organic solvent, followed by slow removal of the organic solvent via reverse-phase evaporation[17]. It was later demonstrated that gradual solvent exchange from organic solvent–water mixtures to water can be utilized to form SLBs on silicon oxide surfaces[18]. In this approach, phospholipids in water–isopropanol (water–IPA) mixtures are deposited on the solid support and then a gradient of water–IPA mixtures (increasing water fraction in 5 mol% increments) are introduced into the measurement chamber. The entire solvent-exchange process takes on the order of 1–2 h. As the water content increases, the phospholipids undergo a series of lyotropic phase transitions, leading to the formation of micelles, monomers, and vesicles in the bulk solution, and the rearrangement of deposited lipid molecules to form an SLB on the silicon oxide surface (Fig. 1). With continuing flow of aqueous buffer, the bulk-phase lipid assemblies are washed away, resulting in a single SLB on the silicon oxide surface.

Although gradual solvent exchange is a potential approach for formation of SLBs, it is rather slow, and we sought to develop a quicker and more robust approach. Therefore, we established the SALB method, which involves lipid deposition in a water-miscible organic solvent, followed by rapid solvent exchange with aqueous buffer[14] (Fig. 2). The direct exchange from organic solvent to aqueous buffer results in a more abrupt series of phase transitions, with a much shorter time scale (<10 min), which is suitable for general fabrication needs. In the course of our early efforts, we discovered that the SALB approach is able to form SLBs not only on silicon oxide surfaces but also on gold surfaces—the latter is one of the most difficult surfaces for the formation of SLBs, and is one on which conventional fabrication methods, such as the vesicle fusion method, cannot be used with conventional zwitterionic lipid compositions[14]. When attempting to replicate our experimental conditions with the gradual

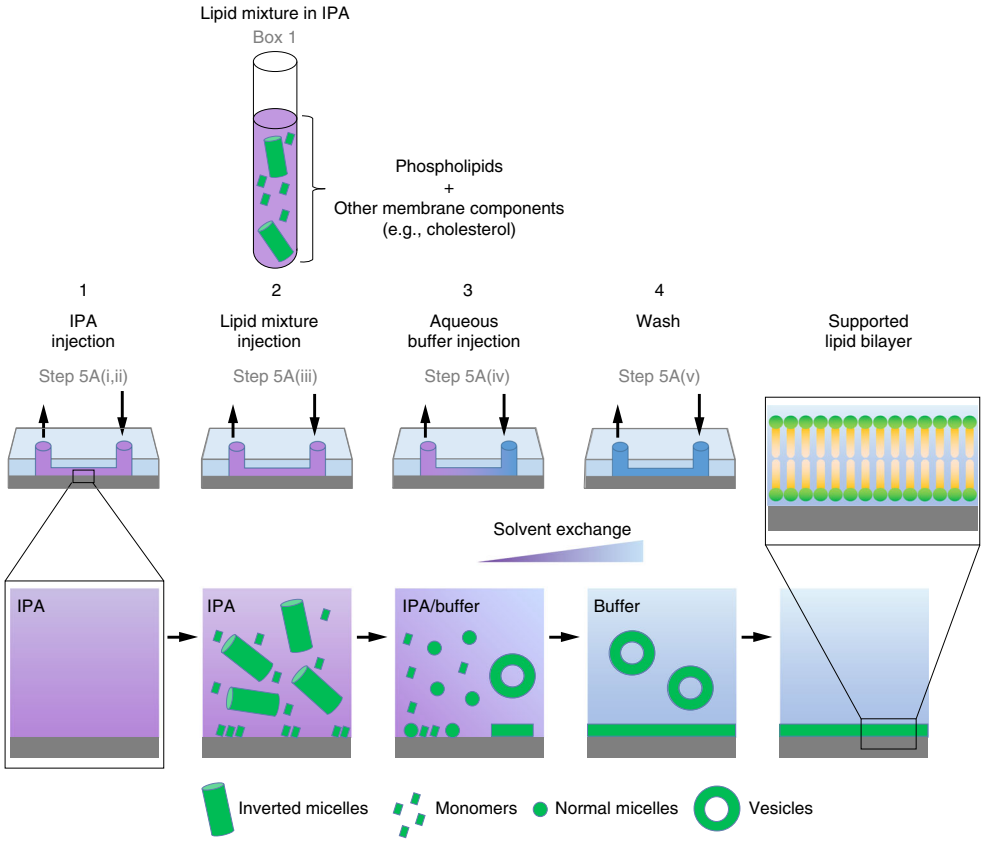

Fig. 2 | Schematic illustration of the stages of the SALB procedure. (1) Water-miscible organic solvent is first introduced. (2) Lipids dissolved in a water-miscible organic solvent (isopropanol (IPA); Box 1) are then added. (3) The bulk solution is then exchanged with aqueous buffer. (4) The measurement chamber is washed with copious amounts of aqueous buffer to remove lipid molecules from the bulk solution, resulting in the formation of a single SLB on the underlying solid support.

solvent-exchange process described above, SLB formation on gold surfaces was not successful, and we realized that successful execution of the SALB procedure requires a detailed understanding of the operating parameters behind the solvent-exchange process (Supplementary Fig. 1). To further understand the SALB protocol's scope and limitations, we attempted the SALB procedure with a series of organic solvents, including IPA, ethanol, methanol, and *n*-propanol. We discovered that IPA yielded the best results, intermediate results were obtained with ethanol and methanol, and inferior SLBs were generated when using *n*-propanol[14]. These findings led us to conclude that not all water-miscible organic solvents are equivalent for use in the SALB protocol and that careful attention to the operating parameters is important for optimal results.

Extending the scope of our characterization efforts, we also systematically tested the effect of bulk lipid concentration on the SLB formation process[19]. During the procedure, the lipids in organic solvent are incubated with the solid support under no-flow conditions before the solvent-exchange step is performed, and we sought to vary the bulk lipid concentration during this incubation period. When using low bulk lipid concentrations, there was an insufficient supply to form a complete SLB during the subsequent exchange process. Rather, incomplete SLB formation occurred, as indicated by the presence of SLB islands with bare, uncoated surface regions between the islands. On the other hand, when using high lipid concentrations, a complete SLB was formed, along with additional nucleated structures protruding from the SLB surface. Such events are solvent specific, and we determined that IPA and *n*-propanol cause the formation of elongated lipid structures, whereas ethanol results in the deposition of vesicle-like structures. Between these two cases, there is an optimal range of bulk lipid concentrations at which complete, high-quality SLB formation occurs. Within this range, SLB formation is highly reproducible and robust. Further investigation revealed that the bulk lipid concentration influences the amount of deposited lipid in equilibrium with the solid support, and hence dictates the density of nucleation sites in the latter stages of the SALB procedure.

Furthermore, the results show that an optimal number of nucleation sites contributes to efficient SLB formation.

Another important parameter is the rate of solvent exchange. If the flow rate is too high, then the SALB procedure results in incomplete SLB formation because there is insufficient lipid supply in the bulk reservoir[14]. This finding was later supported by numerical simulations that showed that the calculated solvent displacement velocity agrees well with the empirically measured SLB formation velocity[20]. Furthermore, an extended phenomenological model determined that lipid monomers are probably the predominant adsorbing species implicated in SLB formation, in agreement with past observations that SLB formation occurs when the water fraction reaches the micelle-to-vesicle transition point[21]. Together, our findings have demonstrated that the SALB procedure can be optimized by controlling the organic solvent type, bulk lipid concentration, and flow rate during the solvent-exchange step. All these parameters are easily controllable, hence making the protocol simple and versatile.

Moving forward, we and others have shown that the SALB procedure is able to form SLBs in a variety of cases in which it is not possible to do so with conventional fabrication methods. In addition to silicon oxide and gold, SLBs can be formed on a wide range of substrates, including chrome, indium tin oxide, titanium oxide, aluminum oxide, graphene, and nanoporous gold[19,22–24]. It is also possible to form SLBs using charged lipid compositions, including monovalent cationic and anionic lipids[25], along with multivalent anionic lipids such as phosphoinositides[26]. The SALB procedure also works with fluid-phase and gel-phase phospholipids alike[19], and can be used to fabricate cholesterol-enriched SLBs[27–29]. When working with lipid compositions containing high cholesterol fractions, it is oftentimes difficult to form SLBs, and the commonly used vesicle fusion method has a typical upper limit of ~20 mol% cholesterol[30]. The Langmuir–Blodgett/Schäfer method is able to form SLBs with higher cholesterol fractions[31]; however, a lack of alignment between domains across the two leaflets[32], along with the exhibition of different phase and structural behaviors in lipid monolayers and bilayers, has been reported for this method[33]. In marked contrast, it is possible to not only form equilibrated SLBs with up to ~60 mol% cholesterol by using the SALB method but also consequently to observe complex biophysical phenomena, such as phase coexistence in the β region of phospholipid–cholesterol mixtures, for the first time in an SLB platform[28]. Depending on the lipid composition, flow geometry, and solid support, minor optimization of the SALB procedure is possible by adjusting the bulk lipid concentration and/or flow rate. These optimization steps are straightforward and provide a clear pathway to achieving high-quality SLBs in all cases.

Applications of the method

The SALB method offers a powerful approach to fabricating SLBs on solid supports that requires minimal preparation and training. For this reason, it should continue to find increasingly wide application among researchers who want to fabricate and utilize SLB platforms. Historically, SLB research has taken place in the chemistry and materials science fields, although there is growing emphasis across a wide range of topics, such as cellular biology, environmental science, and medicine. SLB platforms are broadly useful for studying dynamic processes such as membrane–peptide[34], membrane–protein[35], membrane–antibody[36], and membrane–nanoparticle interactions[37], along with drug development testing[38]. In addition, there is broad interest in incorporating membrane proteins into SLB platforms[39–42].

There is also excellent potential for using the SALB procedure to advance biophysical understanding of SLBs. As mentioned above, SLBs are compatible with a wide range of surface-sensitive measurement techniques, and hence it is a useful cell membrane model for characterizing biophysical phenomena. To date, our understanding of biophysical phenomena in SLBs has been limited by our ability to control the lipid composition of SLBs. For example, it has been difficult to incorporate large fractions of cholesterol or certain types of lipids into the SLB platform. As such, the SALB procedure opens the door to studying SLBs with more diverse compositions, and its fabrication capabilities are far broader than those of existing methods. In the future, these fabrication capabilities should lead to a greater understanding of how biologically relevant membrane compositions are organized[43], including enabling researchers to tackle outstanding questions related to membrane phase separation[44] and molecular arrangements[45].

In addition to fundamental studies, there are a number of emerging applications that utilize SLB platforms, including biosensors[46] and surface coatings[47]. Although SLBs have conventionally been fabricated on silicon oxide surfaces because of material limitations, there is great interest in utilizing

industrially attractive substrates such as gold and titanium oxide. Gold has attractive electrical properties for sensing applications, and it has long been desired to mimic the natural sensing properties of lipid membranes using engineered systems[48]. To this end, ion channel–based sensing platforms have been explored[49,50], and SLBs have been found to have excellent electrical insulating properties[51]. Such motivations have also led to the development of tethered lipid bilayers, which are SLBs that are anchored to an underlying gold surface and have a greater separation distance (hence facilitating a larger ionic reservoir) between the lipid bilayer and the solid support[49,52,53]. In addition, titanium oxide is a popular material for medical implants, and the high biocompatibility of lipid bilayers offers the potential opportunity to coat titanium oxide surfaces as a biomaterial coating[54]. Indeed, zwitterionic lipid bilayers are known to resist nonspecific protein and cell adhesion, among other features[55,56].

Using the SALB procedure, it is also straightforward to incorporate large fractions of functionalized lipids within SLBs, providing an avenue for covalent tethering of peptides and proteins. This approach has proven useful for attaching extracellular matrix (ECM) proteins to SLBs in order to create biomimetic cell culture platforms[57,58] and to study cell–material interactions[59–61]. Furthermore, it is possible to attach peptides[62] and antibodies/proteins[63] to SLBs in order to capture target molecules. This strategy is advantageous because conventionally used zwitterionic SLB platforms are intrinsically non-fouling, and therefore target molecules are captured selectively by molecular recognition. Although nonspecific attachment of biologically relevant peptides and proteins can be achieved in some cases, we have demonstrated particular examples in which covalent attachment of a membrane-associated protein is necessary for subsequent formation of biologically active macromolecular complexes[64]. Another promising application involves cancer diagnostics, in which a clinical-stage SLB platform has been utilized to capture circulating tumor cells with antibody probes[65,66]. Such applications highlight the potential of developing broadly applicable, highly scalable production methods such as the SALB procedure to manufacture SLB platforms.

Overview of the procedure

The SALB procedure is designed to universally form SLBs on a wide range of solid supports. It consists of the following parts: lipid solution preparation (Box 1); microfluidic chamber setup (Steps 1–4); SALB experimental operation (Step 5); optional characterization analyses (Step 6); and optional biofunctionalization (Step 7).

We dissolve lipids in organic solvent and use the lipid solution as the contacting medium for SLB preparation (Box 1). Lipid molecules have different physicochemical properties, such as hydrocarbon chain length, degree of unsaturation, and headgroup charge, so it is important to identify appropriate solvents that solubilize lipids in general. We also discuss different scenarios in which phospholipids and sterols are initially supplied in powder form or chloroform, including recommendations on how to improve lipid solubility when necessary. In addition to lipid solubilization, the selection of an appropriate organic solvent is important because it must be miscible with aqueous buffer. Successful completion of the SALB procedure requires effective mixing between the organic solvent and the running aqueous buffer.

The microfluidic flow chambers are prepared using conventional strategies as part of standalone modules or integrated within measurement devices (Steps 1–4). The quartz crystal microbalance with dissipation monitoring (QCM-D) flow module is used as an example of a measurement device format, and the basic steps are generalizable to other devices as well. In all cases, a critical part of the experimental design is rendering the solid support hydrophilic before experiment. This surface treatment facilitates effective SLB preparation and tight sealing within the chamber. We discuss how oxygen plasma exposure can achieve this goal, although there are other options, such as ultraviolet light exposure. It is also imperative to have a stable, well-controlled flow without air bubbles in order to control the rate of exchange and ensure effective mixing during the SALB procedure.

Once the microfluidic setup is established, we turn to the operation of the SALB protocol (Step 5). The sequence of solution-exchange steps is important for optimal results, not only for successful execution, but also for data interpretation. We use IPA as the exemplary organic solvent. Recommended aqueous buffers and lipid conditions are provided, although minor optimization is probably needed for best results, depending on the flow geometry, material support, organic solvent, and lipid composition. Anticipated measurement responses from QCM-D and fluorescence microscopy experiments are provided as data guidelines. Of particular note, it is useful to have aqueous buffer as the initial reference buffer in order to compare the measurement responses without and with SLB

Box 1 | Lipid solution preparation ● Timing ~15 min

Lipid solution preparation involves mixing lipid samples to the desired molar ratio and mass amount, and transferring them to isopropanol solvent. This box describes solution preparation for lipids that are supplied in the lyophilized powder state or dissolved in chloroform.

1 For sample preparation from lipids in powder form, follow option A. For sample preparation from lipids dissolved in chloroform, follow option B. The operational details of lipid solution preparation are also demonstrated in Supplementary Video 1.

(A) **Lipid solution preparation from powder samples**

(i) For each individual type of lipid, dissolve the appropriate amount of lipid powder in isopropanol in a glass vial to yield a lipid stock concentration of 5–10 mg ml^{-1}. Shake the glass vial with mild agitation until the lipid powder is fully dissolved.

▲ **CRITICAL STEP** For anionic lipids, it is preferable to dissolve them at a stock concentration of 5 mg ml^{-1} in absolute ethanol (see 'Experimental design' section) and incubate the solution at ~50 °C for ~5 min until all the powder is dissolved in the ethanol.

■ **PAUSE POINT** We recommend that lipid stock solutions in organic solvents be prepared at a lipid concentration >1 mg ml^{-1} and used within 2 d of preparation to minimize lipid degradation. The stock solutions should be stored at 4 °C (for up to 1 week).

? TROUBLESHOOTING

(ii) Dilute aliquots of the lipid stock solutions with isopropanol to produce samples with a final lipid concentration of 0.5 mg ml^{-1} or another desired concentration. For lipid mixture solutions, mix appropriate amounts of the respective lipid stock solutions to obtain the desired molar ratio and then dilute the mixture with isopropanol to achieve the target lipid concentration.

(iii) After diluting the sample, ensure homogenization by mixing with gentle pipetting or performing mild vortexing for 10 s. When working with anionic lipids, ethanol may be present in the mixture, and a small fraction of ethanol is acceptable for the SALB protocol.

▲ **CRITICAL STEP** The dilution and mixing steps should be performed immediately before introducing the lipid sample into the measurement chamber. This timing will ensure sample homogeneity and ensure optimal results. Avoid intense or too prolonged vortexing, which may deteriorate lipid suspension properties.

(B) **Lipid solution preparation from chloroform samples**

▲ **CRITICAL** The use of lipid stocks in chloroform is convenient for accurate preparation of lipid mixtures that contain minor fractions of one or more lipids.

(i) Suspend the appropriate volume of lipid stock in chloroform in a glass vial. For lipid mixtures, mix the appropriate volumes of lipid stock to the desired molar ratio in chloroform. The total amount of lipid required for drying depends on the total volume of lipid sample solution needed for the experiment and is typically 5 mg of total lipid.

■ **PAUSE POINT** Lipid stocks in chloroform can be stored for up to one year in a freezer at −20 °C. The vial should be sealed tightly with a cap, preferably with Parafilm wrapping as well, to prevent evaporation of chloroform for long-term storage and to maintain accurate lipid stock concentrations.

! **CAUTION** Ensure that all processes involving chloroform are conducted in a chemical fume hood. Avoid using plastic pipette tips or tubes because chloroform can degrade them. A glass syringe should be used for transferring chloroform solutions between vials.

(ii) Dry the lipid solution with a gentle stream of nitrogen gas while slowly rotating the glass vial at a slightly tilted angle. This will ensure effective, uniform drying on the lower region of the side walls, with greater surface area coverage, and the dry lipid film will appear cloudy and as a partially transparent off-white color.

(iii) Place the glass vials containing dry lipid films in a vacuum desiccator at least overnight.

■ **PAUSE POINT** Dry lipid films can be stored in a vacuum environment for up to one week, and we recommend using the films within 1–2 d to optimally prepare lipid solutions.

(iv) Immediately before introducing the lipid sample into the measurement chamber, add the appropriate amount of isopropanol to solubilize the dry lipid film, with a final lipid concentration of 0.5 mg ml^{-1} or another desired concentration.

(v) Ensure homogenization by mixing the dispersed lipid sample with gentle pipetting or performing mild vortexing for 10 s.

▲ **CRITICAL STEP** The dilution and mixing steps should be performed immediately before introducing the lipid sample into the measurement chamber. This timing will ensure sample homogeneity and ensure optimal results. Avoid intense or too prolonged vortexing, which may deteriorate lipid suspension properties.

coating (i.e., before and after the SALB procedure is conducted) while keeping other parameters such as the bulk liquid condition equivalent.

Additional steps in the procedure are used to characterize the quality of SLBs prepared by the SALB protocol (Step 6). Three main types of characterization are introduced: nonspecific protein adsorption for measuring the fractional surface coverage of an SLB on a solid support (Step 6A), specific protein binding to particular lipid headgroups in order to quantify lipid composition (Step 6B), and sterol removal by methyl-β-cyclodextrin (MβCD) in order to quantify the cholesterol

fraction in an SLB (Step 6C). Depending on the experimental objective, these characterization steps are important for SLB evaluation and have proven useful for demonstrating the merits of the SALB procedure as compared with other conventional fabrication methods. These steps are also useful for optimizing the SALB protocol for the particular system under consideration. For example, when using the SALB protocol, we have typically observed that the molar fraction of cholesterol in the SLB is slightly higher than the molar fraction of cholesterol in the input mixture[27].

The conventional SALB procedure can also be expanded by including additional biofunctionalization steps (Step 7). Such options are directly linked to the expanded fabrication capabilities afforded by the SALB method and lead to opportunities for incorporating tethering lipids and signaling lipids. In one example, we demonstrate how ECM proteins can be attached to headgroup-functionalized lipids within the SLB under specific chemical conditions[67] (Step 7A). We demonstrate protein attachment using ethylcarbodiimide hydrochloride–*N*-hydroxysuccinimide (EDC–NHS) chemistry with phosphoethanolamine-*N*-(glutaryl) lipids, and another popular attachment scheme involves coupling of His-tagged proteins to nickel-chelating lipids[68–73]. Other possibilities include coupling based on nucleic acid hybridization[74] and biotin–streptavidin binding[75]. In another example, we discuss how phosphoinositide lipids can be incorporated into an SLB as a proxy for monitoring the catalytic activity of kinase enzymes[26] (Step 7B). A critical aspect of these biofunctionalization steps is that the SALB procedure enables large fractions of headgroup-functionalized lipids to be incorporated within an SLB.

Comparison with other methods

Over the years, numerous strategies have been developed to fabricate SLBs on solid supports. Most of the strategies are aimed at either Langmuir-type transfer of preformed lipid films to a solid support[76,77] or promoting the molecular self-assembly of lipids contacting a solid support[78]. Within this scope, one of the most popular strategies involves the adsorption and spontaneous rupture of lipid vesicles (termed 'vesicle fusion') on a solid support[79,80]. On silicon oxide-based materials, lipid vesicles oftentimes adsorb until reaching a critical surface coverage, followed by spontaneous rupture[81,82]. As a result, the adsorbed lipids reassemble on the surface, resulting in the stable formation of an SLB that is separated from the solid support by a thin, nanometer-scale hydration layer[83,84]. Although the basic steps of the vesicle fusion method are straightforward, successful SLB formation depends on numerous factors, chief among them vesicle properties. Producing vesicles suitable for high-quality SLB formation is a delicate art that requires precision control over size, lamellarity, lipid composition, and solution conditions[85]. Using this approach, it is also challenging to incorporate biological components, such as sterols, that rigidify lipid vesicles[86], as well as signaling lipids that impart high negative membrane surface charge[87]; such factors hinder spontaneous rupture of adsorbed lipid vesicles, limiting the scope of possible SLB compositions.

In addition, adsorbed vesicles rupture on only a narrow range of material supports; on other surfaces, vesicles typically either adsorb and remain unruptured or do not adsorb at all (see ref. [82] and references therein). The empirical challenge of the vesicle fusion approach is beset by the conundrum that the interaction energy needed to stabilize an SLB on the surface is smaller than the interaction energy needed to induce the rupture of an adsorbed vesicle[88]. Only a few solid supports, in particular, silicon oxide-based materials, have suitable properties to facilitate the spontaneous rupture of adsorbed vesicles. As such, the vesicle fusion method requires skilled vesicle preparation and works with only a narrow range of material supports and lipid compositions. Within this context, it should be emphasized that the SALB method requires only a minimal degree of attractive lipid–substrate interactions to successfully form SLBs on various substrates. This is a key advantage over the vesicle fusion method because there is no high-energy requirement to induce the rupture of adsorbed vesicles, and this is principally why the SALB method works on a wider range of substrates. For example, the SALB procedure is able to form SLBs on silicon oxide and gold surfaces, whereas the conventional vesicle fusion procedure works only on silicon oxide and adsorbed vesicles remain intact on gold. This performance contrast between the SALB and vesicle fusion methods is exemplified in Fig. 3.

Although advanced fabrication strategies such as air-bubble collapse[89] and dip-pen nanolithography[90,91] have been developed to form SLBs under highly specific conditions, their successful application remains limited to specific instances, and large-scale patterning of an entire surface is difficult to achieve with these approaches. On the other hand, spin-coating[92] is capable of producing a fully coated surface, although it is typically used for forming homogeneous bilayer stacks with defined

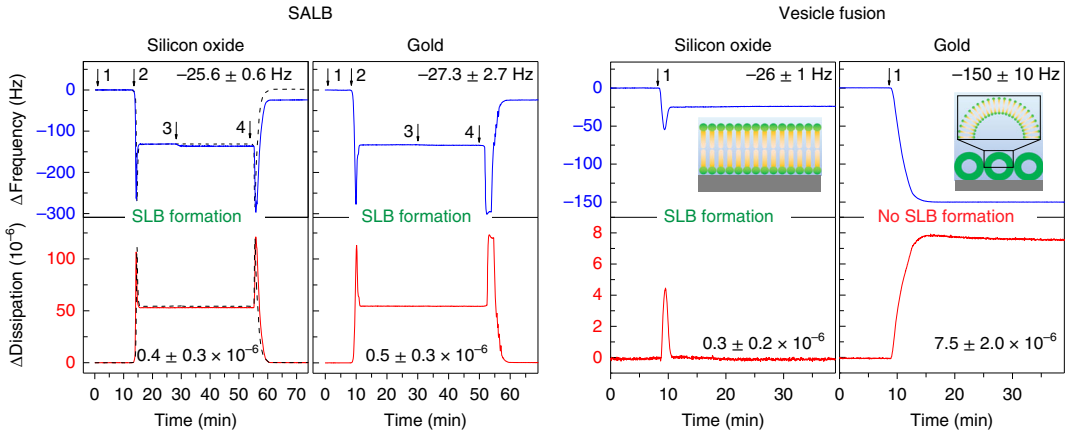

Fig. 3 | Comparison of SALB and vesicle fusion methods on silicon oxide and gold surfaces. Quartz crystal microbalance–dissipation (QCM-D) data show frequency (top, blue) and energy dissipation (bottom, red) shift responses. For the SALB procedure (left-hand panels), arrows indicate (1) buffer addition, (2) isopropanol exchange, (3) DOPC lipid-in-isopropanol exchange, and (4) buffer exchange. Dashed lines show a control experiment without lipid. For the vesicle fusion procedure (right-hand panels), DOPC lipid vesicles were added at $t = 10$ min (1). The measurement values in each panel show the corresponding final frequency and energy dissipation shifts after SLB formation is complete. Data are reported as mean ± standard deviation. Adapted with permission from ref. [14], American Chemical Society.

thicknesses, rather than single, uniform bilayers. In a few cases when spin-coating has been conducted with low lipid concentrations, it has been possible to form lamellar-phase, single lipid bilayers on mica surfaces in dry air conditions[93,94]. Lipid wetting[95] is another useful technique, whereby crystalline lipid is hydrated with aqueous solvent in order to promote lipid spreading and SLB formation on a hydrophilic surface, including silicon oxide-based ones. Some caveats are that it can be difficult to coat an entire surface because of pinning sites and that the spreading mechanism is sensitive to the lipid composition and substrate properties[96]. Table 1 compares the SALB method with other fabrication methods.

Level of expertise needed to implement the protocol

The protocol can be completed in a standard wet lab without any particular level of expertise. Some instruction is required to learn about handling lipids in organic solvents and in aqueous buffers, along with basic steps for substrate cleaning, microfluidic chamber assembly, and pump handling. In our experience, a person can master the different parts of the basic protocol within a few days, and such capabilities would be sufficient for operating SLB-based assays in a variety of application settings as well. Additional time is required for learning how to use accompanying analytical instrumentation for SLB characterization. Such measurement techniques would be particularly beneficial for biophysical investigations in advanced application settings.

Experimental design

Organic solvent type

In this protocol, we use IPA as the typical organic solvent of choice. However, there are other suitable options, including ethanol and methanol, and a key requirement is that the organic solvent be miscible with aqueous buffer. When working with anionic lipids, it is sometimes preferable to initially dissolve them in ethanol rather than IPA, which we typically use for zwitterionic and cationic lipids, along with sterols. In such cases, the resulting lipid mixtures used during the incubation step may contain a minor fraction of ethanol along with a major fraction of IPA. In our experience, the combination of IPA and ethanol to prepare lipid solutions when working with mixtures of zwitterionic and anionic lipids is suitable for successful SLB preparation. Nevertheless, users should check the performance of different lipid mixtures of their choice in order to verify compatibility with the SALB procedure.

Lipid concentration

It is generally recommended to use bulk lipid concentrations in the range of 0.1–0.5 mg ml^{-1}. Above this range, additional nucleation events can occur on the SLB surface. Below this range, there may be insufficient lipid in the bulk reservoir to ensure complete SLB formation. The specific details depend on the system under consideration and may require slight optimization. In our experience, we have

Table 1 | Comparison of SLB fabrication methods

Method	Basic principle	Experimental considerations	Refs.
Langmuir–Blodgett/ Langmuir–Schäfer deposition	Transfer of lipid films from the air–solution interface to the air–solid interface on a solid support	Requires Langmuir trough setup Involves successive transfer of lipid monolayers Lack of alignment between domains in the two leaflets	76,77
Bubble-collapse deposition	Controlled rupture of individual vesicles on a solid support in an aqueous environment	Requires vesicle preparation and precise rupture action It is difficult to coat large areas	88,89
Dip-pen nanolithography	Transfer of lipid molecules from a lipid solution droplet at the atomic force microscope tip to the solid support in a humidity-controlled environment	Requires use of atomic force microscope It is difficult to coat large areas	90,91
Spin coating	Rotation-induced spreading of lipid molecules on a solid support from a centrally deposited lipid mixture in organic solvent	It is suitable for forming lipid multilayers with defined thicknesses It is difficult to control formation of a single lipid bilayer film	92–94
Lipid wetting	Spreading of a lipid layer from a point source of deposited crystalline lipid upon hydration in an aqueous solvent	It is difficult to coat large areas due to pinning sites Spreading mechanism is sensitive to lipid composition and substrate properties	95,96
Vesicle fusion	Spontaneous rupture of adsorbed lipid vesicles on a solid support in an aqueous environment	Requires vesicle preparation Works on only a limited range of substrates and lipid compositions	79–81
SALB	Spontaneous self-assembly of lipid molecules on a solid support triggered by exchanging from organic solvent to aqueous solvent	Compatible with basic microfluidics Straightforward optimization of lipid concentration and flow conditions	14,19,27

elected to use 0.5 mg ml^{-1} when working with 1,2-dioleoyl-*sn*-glycero-3-phosphocholine (DOPC) lipids but found more reliable results when using 0.3 mg ml^{-1} for DOPC–cholesterol mixtures, depending on the system.

Lipid composition

One advantage of the SALB protocol is that it is able to form SLBs from a wide range of lipid compositions, including mixtures of phospholipids and sterols. In this protocol, we use zwitterionic DOPC lipid as the main example and also refer to other cases in which different lipid compositions might be suitable, including DOPC–cholesterol systems. In general, the SALB procedure follows the same steps independent of the lipid composition, and we have successfully worked with numerous lipid compositions, including the following headgroup examples: phosphatidylcholine, phosphatidylglycerol, phosphatidylserine, ethylphosphatidylcholine, phosphatidylinositol, and phosphoethanolamine-*N*-(glutaryl) with various combinations of hydrocarbon chains (typically, C16/C16, C18:1/C16, or C18:1/C18:1). We have successfully used lipid mixtures with up to 50 mol% charged lipid or up to 60 mol% cholesterol. There are many other possibilities, and users should empirically optimize the SALB procedure with the lipid composition of choice, especially when conducting experiments on different solid supports. Also, due attention should be paid to effective solubilization when working with charged lipids, as proper mixing of different lipids in the bulk solution is critical for efficient SLB preparation with the desired composition.

Measurement chamber

The SALB protocol is designed to form SLBs within enclosed measurement chambers to promote solvent exchange under controlled conditions. In our protocol, we demonstrate successful SLB formation using a commercially available, polymer-based microfluidic chamber (Step 4A) that has a volume of ~30–100 µl, depending on the channel configuration, and with a stainless steel measurement chamber of a commercial QCM-D instrument (Step 4B) that has a volume of ~60 µl[97]. It is possible to use other measurement chambers with different flow geometries, material compositions, and volumes, and empirical optimization of the operating parameters is warranted, depending on the system under consideration. It is important to ensure solvent compatibility with the measurement chamber of choice, as well as with associated tubing.

Flow conditions

We recommend use of a peristaltic pump to control the flow rate because it is necessary to maintain a stable and constant flow speed during the exchange steps. Indeed, effective SLB formation requires an optimized balance of the lipid concentration and flow rate, so proper maintenance of the latter is critical. Also, although the time scale of SLB production is relatively short, the flow volume is relatively large, in order to ensure complete solvent exchange. Therefore, a peristaltic pump is preferable to a volume-limited syringe pump. Alternatively, it is possible to use a syringe pump or pipetting, depending on the application, although empirical optimization of the operating parameters, especially the lipid concentration and exchange step (e.g., flow speed and duration), is warranted.

Materials

Reagents

- Deionized water (resistivity of >18 MΩ·cm at 25 °C)
- Isopropanol (IPA; Merck, cat. no. 278475) **! CAUTION** IPA is flammable and can cause eye irritation. Keep away from open flames and keep the container tightly closed when not in use.
- Ethanol (Merck, cat. no. 1009832511) **! CAUTION** Ethanol is flammable and can cause eye irritation. Keep away from open flames and keep the container tightly closed when not in use.
- SDS (Merck, cat. no. L3771)
- Methyl-β-cyclodextrin (MβCD; Merck, cat. no. C4555)
- Annexin A5 (Merck, cat. no. SRP8026)
- *N*-hydroxysulfosuccinimide sodium salt (sNHS; Alfa Aesar, cat. no. H52795)
- 1-(3-Dimethylaminopropyl)-3-ethylcarbodiimide hydrochloride (EDC; Alfa Aesar, cat. no. A10807)
- Anti-PtdIns(4)P IgM (anti-PI4P IgM; Echelon Biosciences, cat. no. Z-P004)
- DL-DTT (Merck, cat. no. D0632)
- EGTA (Merck, cat. no. E3889)
- Adenosine 5′-triphosphate disodium salt hydrate (ATP; Merck, cat. no. A2383)
- Tris (VWR, cat. no. 97061-794)
- PBS (1×; HyClone, cat. no. SH30256.01)
- HEPES ($C_8H_{18}N_2O_4S$; Merck, cat. no. H3375)
- Sodium chloride (NaCl; Merck, cat. no. 746398)
- Calcium chloride ($CaCl_2$; Merck, cat. no. 102391)
- Magnesium chloride ($MgCl_2$; Merck, cat. no. 814733)
- Hydrochloric acid (HCl; Merck, cat. no. 100317) **! CAUTION** HCl is corrosive and can cause burns. Always wear appropriate personal protective equipment (including a lab coat, gloves, and safety goggles) when handling the chemical.
- Sodium hydroxide (NaOH; Merck, cat. no. S5881) **! CAUTION** NaOH is corrosive and can cause burns. Always wear appropriate personal protective equipment (including a lab coat, gloves, and safety goggles) when handling the chemical.
- Nitrogen gas (Leeden National Oxygen, cat. no. CGC024)

Lipids

- 1,2-Dioleoyl-*sn*-glycero-3-phosphocholine (DOPC; Avanti Polar Lipids, cat. no. 850375)
- 1,2-Dioleoyl-*sn*-glycero-3-phospho-L-serine (sodium salt) (DOPS; Avanti Polar Lipids, cat. no. 840035)
- 1,2-Dioleoyl-*sn*-glycero-3-ethylphosphocholine (DOEPC; Avanti Polar Lipids, cat. no. 890704)
- 1,2-Dioleoyl-*sn*-glycero-3-phosphoethanolamine-*N*-(lissamine rhodamine B sulfonyl) (ammonium salt) (Rh-PE; Avanti Polar Lipids, cat. no. 810150)
- 1,2-Dipalmitoyl-*sn*-glycero-3-phosphoethanolamine-*N*-(glutaryl) (sodium salt) (DP-NGPE; Avanti Polar Lipids, cat. no. 870245)
- Cholesterol (Avanti Polar Lipids, cat. no. 700000)
- L-α-phosphotidylinositol (PI; Avanti Polar Lipids, cat. no. 840024)
- Phosphatidylinositol 4-phosphate diC16 (PI4P; Echelon Biosciences, cat. no. P-4016)
- Phosphatidylinositol 4-kinase beta (PI4Kβ; Thermo Fisher Scientific, cat. no. PR9008A) **▲ CRITICAL** It is recommended to use high-purity phospholipids (>90%). If natural extracts are used, further optimization may be required, depending on the lipid composition. Additional purification steps may be necessary if results are unsatisfactory.

Equipment

- Gas-tight glass syringes, 500 µl volume (Hamilton, cat. no. 81230)
- pH meter (Fisher Scientific, model no. Accumet Basic AB15)
- Analog vortex mixer (VWR, Vortexer Mini 230V, model no. 58816-123)
- Analytical mass balance (Boeco, model no. BXX 22)
- Oxygen plasma cleaner (Harrick Plasma, model no. PDC-002)
- QSense Analyzer (QCM-D) instrument (Biolin Scientific)
- Inverted microscope (Nikon, Eclipse Ti-E, model no. TI-DH)
- Mercury light source (Nikon, Intensilight, model no. C-HGFIE)
- Electron-multiplying charge-coupled device (EMCCD) camera (Andor Technology, model no. iXon3-897)
- Single-mode laser source (532 nm, 100 mW; Coherent, OBIS, model no. OBIS 532-100 LS)
- CFI Apochromat TIRF 60× oil-immersion objective lens (numerical aperture (NA) 1.49) (Nikon, model no. MRD01691)
- Peristaltic pump (Ismatec, model no. Reglo Digital MS-4/6)
- Tweezers (Ideal-tek, model no. 2A.SA.6)

Consumables

- Syringe filters (0.2-µm pore diameter; VWR, cat. no. 28145-475)
- QCM-D sensor chips with silicon oxide, titanium oxide, aluminum oxide, and gold coatings (Biolin Scientific, cat. nos. QSX303, QSX310, QSX309, and QSX301)
- Ismatec SC0307 three-stop, Pharmed BPT tubing (for pump), with 0.76-mm i.d. (Cole-Parmer, cat. no. EW-95714-24)
- Teflon (polytetrafluoroethylene) tubing (for inlet and outlet of the microfluidic flow chamber and the QCM-D flow module) with 0.76-mm i.d. and 1.59-mm o.d. (Vici, cat. no. TTF130-10M)
- Polypropylene nuts, chlorotrifluoroethylene ferrules with 1/16-inch tube end fittings (Vici, cat. no. CFL-1W)
- Glass coverslips (no. 1.5H, 25 mm × 75 mm; ibidi, cat. no. 10812)
- sticky-Slide VI 0.4 microfluidic chip for six channels (ibidi, cat. no. 80608)
- sticky-Slide I Luer microfluidic chip for one channel (ibidi, cat. no. 80168)
- Elbow Luer connector (ibidi, cat. no. 10802)
- TRITC filter set (Chroma)
- Parafilm (Bemis, cat. no. PM996)

Software

- QSense Dfind v.1.2 (Biolin Scientific, https://www.biolinscientific.com/qsense/software/)
- NIS-Elements AR v.4.0 (Nikon, https://www.nikon.com/products/microscope-solutions/support/download/software/imgsfw/)
- MATLAB v.R2018b (MathWorks, https://www.mathworks.com/downloads/)

Reagent setup

Tris–NaCl buffer

Prepare Tris–NaCl buffer (10 mM Tris (pH 7.5), 150 mM NaCl) by dissolving 1.21 g of Tris and 8.76 g of NaCl in 1 liter of deionized water. Adjust the solution pH to 7.5. After the pH is adjusted, filter the buffer and then dispense it into a sealed glass bottle. Store the buffer at room temperature (20–25 °C). For best results, avoid using buffers that have been stored for >2 months.

Tris–NaCl–$CaCl_2$ buffer

Prepare Tris–NaCl–$CaCl_2$ buffer (10 mM Tris (pH 7.5), 150 mM NaCl, 2 mM $CaCl_2$) by dissolving 1.21 g of Tris, 8.76 g of NaCl, and 222 mg of $CaCl_2$ in 1 liter of deionized water. Adjust the solution pH to 7.5. After the pH is adjusted, filter the buffer and then dispense it into a sealed glass bottle. Store the buffer at room temperature. For best results, avoid using buffers that have been stored for >2 months.

HEPES–NaCl buffer

Prepare HEPES–NaCl buffer (10 mM HEPES (pH 5.5), 100 mM NaCl) by dissolving 2.36 g of HEPES and 5.84 g of NaCl in 1 liter of deionized water. Adjust the solution pH to 5.5. Once the pH is set to

5.5, dispense the buffer into a sealed glass bottle. Store the buffer at room temperature. For best results, avoid using buffers that have been stored for >2 months.

Kinase buffer

Prepare kinase buffer (20 mM Tris (pH 7.5), 5 mM $MgCl_2$, 2 mM DTT, 0.5 mM EGTA, 100 μM ATP) by dissolving 2.42 g of Tris, 476 mg of $MgCl_2$, 309 mg of DTT, 190 mg of EGTA, and 55.1 mg of ATP in 1 liter of deionized water. Adjust the solution pH to 7.5 and store the buffer at 4 °C. For best results, it is recommended to prepare fresh buffer on the day of the experiment.

SDS solution

Dissolve 10 g of SDS in 1 liter of deionized water to prepare a 1% (wt/vol) SDS solution. Mix well to ensure that the SDS has fully dissolved. Allow the solution to rest and wait for bubbles to disappear. Afterward, dispense the SDS solution into a sealed glass bottle. Store the solution at room temperature. The SDS solution can be used as long as there are no visible signs of contamination or precipitation. For best results, it is recommended to use the SDS solution within 1 month.

Lipid solutions

Lipid solutions can be prepared as described in Box 1 (see also Supplementary Video 1), either from powder samples (Step 1A) or from chloroform samples ((Step 1B). Stock solutions can be prepared in advance, whereas lipid mixture samples should be prepared immediately before introducing the lipid sample into the measurement chamber in Step 5.

Equipment setup

Peristaltic pump and tubing

While the pump is in off mode, fix the flexible pump tubing to the cassette and snap the cassette onto the roller-head of the pump. Ensure that the tubing is straight (not twisted) and that the correct tubing diameter is selected in the pump settings. Connect the flexible pump tube to a Teflon tube, which in turn is attached to the inlet port of the microfluidic chamber. Connect a separate Teflon tube to the outlet port of the microfluidic chamber. The flow direction of the pump should be set so that the liquid solution flows from the inlet port to the outlet port. For best results, it is preferable to regularly use new tubing because of wear-and-tear, stretching, and possible solvent effects.

QCM-D instrument

The experiments are conducted using a QSense Analyzer instrument, and liquid sample is introduced by a peristaltic pump. QCM-D measurements track changes in the resonance frequency (Δf) and energy dissipation (ΔD) signals of material support–coated, oscillating quartz crystal sensor chips in response to thin film mass adsorption. The temperature is set to ~25 °C, and the experimental operation is controlled by the QSense Dfind software package. It is important to run experiments under temperature control to minimize thermal drift, which will affect signal stability. Before the experiment, the sensor chips' resonance frequency and dissipation values should be checked in Tris–NaCl buffer at several overtones. The values should agree well with reference values. Once each experiment is completed, clean the instrument by sequentially flowing 1% (wt/vol) SDS solution for at least 15 min, water for 10 min, and ethanol for at least 15 min at a flow rate of ≥500 μl min^{-1}. During experiments and cleaning steps, stop the pump when exchanging solutions in order to avoid the introduction of air bubbles. After ethanol rinsing, air-dry the tubing and chambers by keeping the pump switched on at the same flow rate for at least 2 min, without injecting any solution. Afterward, disassemble the flow modules and remove the sensor chips.

Inverted epifluorescence microscopy

The experiments are conducted using an inverted Eclipse Ti-E microscope, which is well suited for integration with microfluidic flow chambers. The microscope is equipped with a high-NA objective (60×/1.49 NA) with a short working distance (0.12 mm). This allows a high amount of light into the lens and provides a shallow depth of field in which to observe SLBs. For high-NA objectives, glass thickness variations of only a few micrometers can lead to appreciable optical aberrations. Thus, it is critical to use coverslips with appropriately thin and smooth glass (~0.200 ± 0.005-mm thickness) and to rotate the correction collar of the objective to achieve optimal resolution and contrast. In our setup, we use a mercury light source equipped with a TRITC filter set. Depending on the experimental

objective, it is possible to use bare glass coverslips or material support–coated ones, such as titanium oxide–coated glass coverslips.

Fluorescence recovery after photobleaching (FRAP)

A single-mode laser source of 532 nm (100 mW) is used for photobleaching experiments. Images are captured using a high-resolution, thermoelectric-cooled EMCCD camera with a resolution of 512 pixels × 512 pixels. The entire microscope setup rests on an antivibration stage, and experiments are conducted at 24 ± 1 °C in a dark room. All imaging operations are controlled via the NIS-Elements AR software, which is capable of regulating shutter speed with millisecond precision to minimize light exposure and to perform programmed time-lapse imaging. Note that the protocol can also be performed using alternative inverted epifluorescence microscopes and other microscopes with suitable specifications, although some level of optimization is needed, depending on the setup and application.

Procedure

Microfluidic chamber setup ● Timing ~15 min

1 Rinse the material support substrate (e.g., coverslip, wafer, or sensor chip coated with the appropriate substrate material, such as silicon oxide, gold, titanium oxide, or graphene) with 1% (wt/vol) SDS solution, water, and ethanol in sequential order.

2 Dry the substrate with a gentle stream of nitrogen gas. We recommend using blunt tweezers to hold the substrate by its edge during the washing and drying process.

3 Remove any residual organic contaminants on the substrate surface by exposing the surface to oxygen plasma treatment for ~1 min. After oxygen plasma treatment is completed, immediately proceed to Step 4 in order to minimize exposure to air contaminants.

▲ CRITICAL STEP The substrate should be treated with oxygen plasma immediately before the microfluidic chamber is assembled to ensure that the surface remains clean and hydrophilic during the subsequent experiment.

4 Prepare the microfluidic chamber. For chamber setup with conventional microfluidics, follow option A. For chamber setup with a QCM-D instrument, follow option B.

(A) **Chamber setup with conventional microfluidics**

▲ CRITICAL The operational details for assembling a microfluidic chamber using conventional microfluidics are also demonstrated in Supplementary Video 2.

(i) Assemble the microfluidic chamber by attaching the oxygen plasma–treated glass coverslip to a sticky-Slide microfluidic chip (refer to Fig. 4a). For the assembly of a single-channel microfluidic chamber, we recommend the use of a sticky-Slide I Luer microfluidic chip. For the assembly of a multichannel microfluidic chamber, we recommend the use of a sticky-Slide VI 0.4 microfluidic chip.

▲ CRITICAL STEP This step should be performed immediately after the glass coverslip is treated with oxygen plasma (Step 3). Ensure that the oxygen plasma–treated surface of the coverslip is facing the self-adhesive underside of the sticky-Slide chamber. If another type of polymer-based microfluidic chip without an adhesive layer is used, then the microfluidic chip itself should also be treated with oxygen plasma before the experiment in order to render its surface hydrophilic for sealing purposes.

? TROUBLESHOOTING

(ii) Fill the flow channel(s) with Tris–NaCl buffer by pipetting the buffer into the outlet port until the flow channel is completely filled with buffer and a convex meniscus is observed at the top of the inlet port (refer to Fig. 4b). For the multichannel microfluidic chamber, all channels should be filled with buffer in this step.

▲ CRITICAL STEP Filling the channels with buffer is essential to ensuring the chamber is well sealed before the experiment and to maintaining the surface hydrophilicity, especially when a multichannel microfluidic chamber is used, as all chambers are not used simultaneously. Ensure that there is no air bubble or liquid leakage in the assembled microfluidic chamber when buffer is added. For optimal results, we recommend first filling the chamber with Tris–NaCl buffer, rather than directly proceeding to the use of IPA solution.

(iii) Connect the Teflon tubing to the three-stop flexible tubing and fix an elbow connector to the open end of the Teflon tubing (this constitutes the outlet tubing fixture). Dip the elbow

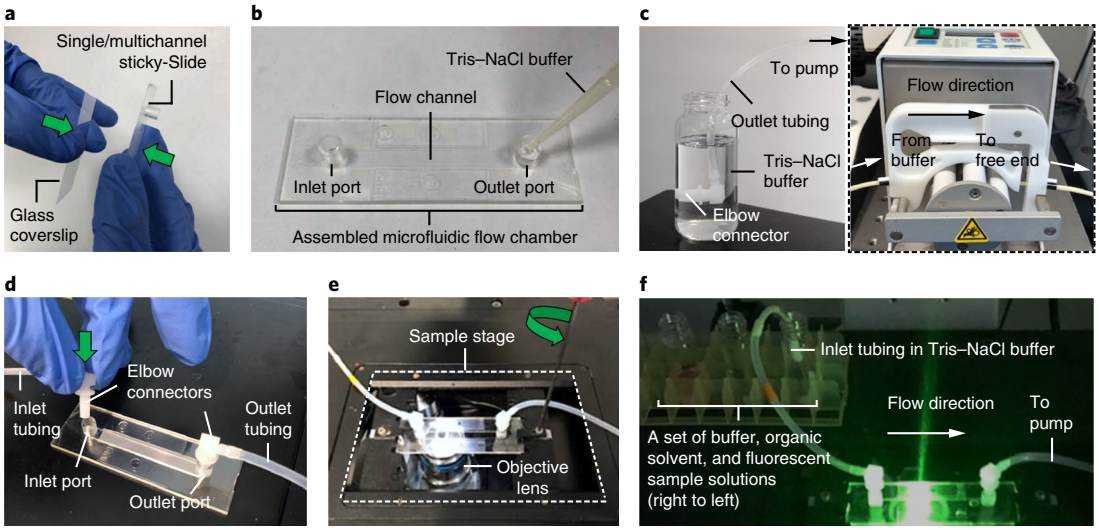

Fig. 4 | Microfluidic chamber assembly and attachment in microscope setup. a, Attach an oxygen plasma-treated glass coverslip to the microfluidic chip. **b**, Fill the flow channel(s) with Tris-NaCl buffer. **c**, Connect the tubing and begin running the peristaltic pump to initiate buffer flow. **d**, Stop the pump after the tubing is filled with buffer and connect the tube end to the outlet port of the microfluidic chamber. **e**, Secure the microfluidic chamber to the sample stage of the microscope and carefully screw in the holding clips. **f**, Dip the free end of the inlet tubing into a separate vial of buffer and restart the pump in the opposite flow direction until all tubing is filled. A practical example of applying these steps is provided in Supplementary Video 2.

connector into a bottle of Tris–NaCl buffer. Attach the three-stop flexible tubing to the peristaltic pump.

▲ **CRITICAL STEP** Ensure that the elbow connectors are fixed tightly to the chamber in order to prevent the generation of air bubbles during the exchange process.

(iv) Start the pump in order to draw buffer from the elbow connector into the free end of the flexible tubing (refer to Fig. 4c). Once the buffer begins to drip out of the free end of the tubing (i.e., the entire outlet tubing fixture has been completely filled with buffer), stop the pump.

(v) Remove the elbow connector from the bottle of Tris–NaCl buffer and slot it into the outlet port of the microfluidic chamber. Connect another elbow connector to the inlet tubing and slot it into the inlet port of the microfluidic chamber, which was pre-filled with buffer in Step 4A(ii) (refer to Fig. 4d).

(vi) After checking that all the connected tubes are filled with buffer, reverse the flow direction and restart the pump. Once the buffer exits the free end of the inlet tubing, stop the pump.

▲ **CRITICAL STEP** Ensure that there is no buffer leakage. If leakage occurs, then adjust the tubing until there is no leakage and try different flow rates to verify that there is stable flow.

▲ **CRITICAL STEP** If the microfluidic chamber is being attached to a microscope stage, first place a drop of immersion oil on the objective lens, secure the microfluidic chamber to the sample stage of the microscope, and then carefully screw in the holding clips. The glass side of the microfluidic chamber should be in contact with the immersion oil on the objective lens (refer to Fig. 4e).

? TROUBLESHOOTING

(vii) Dip the free end of the inlet tubing into a separate vial of Tris–NaCl buffer (refer to Fig. 4f). Switch back the flow direction and restart the pump and run it until the buffer exits the free end of the outlet tubing. Maintain the flow at a flow rate of 100–1,000 μl min^{-1}. Proceed to Step 5A(i) for SLB fabrication with fluorescence microscopy monitoring.

▲ **CRITICAL STEP** Visually inspect the tubing and the chamber reservoir to ensure that no air bubbles were introduced into the measurement chamber and that the buffer drips out of the outlet tubing at regular intervals.

? TROUBLESHOOTING

(B) **Chamber setup with QCM-D instrumentation**

(i) Mount the QCM-D sensor chip in the flow module, resting on the O-ring support, and carefully screw the contact block onto the flow module.

! CAUTION The mounted sensor chip may be subjected to uneven pressure when the contact block is screwed in in a lopsided manner, and this pressure may cause the sensor chip to break. Avoid completely screwing in one side of the contact block before screwing in the other side. Instead, alternate between the two sides while gradually tightening the screws, or tighten both sides simultaneously to maintain equal pressure on the mounted sensor chip.

▲ CRITICAL STEP This step should be performed immediately after oxygen plasma cleaning of the QCM-D sensor chip (Step 3). Before mounting the sensor chip, ensure that both the sensor chip and the flow module are completely dry. Also ensure that there is no residual liquid trapped around the O-ring.

(ii) Attach the assembled flow module to the electrical contacts within the instrumental platform.

(iii) Start the peristaltic pump to inject Tris–NaCl buffer into the measurement chamber at a flow rate of ~100 µl min^{-1}.

▲ CRITICAL STEP This step is performed before the QCM-D signals are acquired, in order to prefill the tubing with buffer. Visually check the tubing to ensure that no air bubbles were introduced into the measurement chamber and that buffer regularly drips from the outlet tubing.

? TROUBLESHOOTING

(iv) Start the measurement run and continue to flow buffer until the frequency and energy dissipation values have stabilized. Maintain a continuous flow to introduce fresh buffer at a constant speed. As a rule of thumb, the values have stabilized when the frequency fluctuates <1 Hz and the dissipation fluctuates $<0.2 \times 10^{-6}$ over a 10-min interval.

▲ CRITICAL STEP Ensure that Tris–NaCl buffer is used for SLB fabrication. Tris–NaCl buffer is the optimal buffer for fabrication of high-quality homogeneous SLBs using the SALB method. After SLB fabrication, other biological buffers can be used, depending on the experimental requirements.

SLB fabrication ● Timing ~30 min

5 After the microfluidic chamber has been set up, SLB fabrication can proceed. For SLB fabrication with fluorescence microscopy monitoring, follow the steps in option A. For SLB fabrication with QCM-D monitoring, follow the steps in option B.

(A) **SLB fabrication with fluorescence microscopy monitoring**

▲ CRITICAL All steps in this section should be conducted in a dark room to minimize photobleaching of the fluorescently labeled lipid molecules.

(i) Continuing Step 4A(vii), introduce IPA through an inlet port at a flow rate of 100 µl min^{-1} for 10 min to completely fill the chamber with IPA.

▲ CRITICAL STEP Check that no air bubbles are formed when the IPA mixes with, and subsequently replaces, the buffer.

? TROUBLESHOOTING

■ PAUSE POINT The flow can be maintained at 100 µl min^{-1} while lipid solutions are being freshly prepared (see 'Reagent setup' section and Box 1). Maintaining the flow for >10 min should not affect the bilayer quality.

(ii) Ensure a constant and stable flow speed when the IPA is added to the microfluidic chamber, and adjust the focal plane and field of view to image the glass coverslip surface.

(iii) Flow the 0.5 mg ml^{-1} lipid solution in IPA into the microfluidic chamber at a flow rate of 50 µl min^{-1} for at least 1 min to ensure complete exchange without dilution effects. The lipid solution should contain a fluorescent lipid, preferably 0.5 mol% Rh-PE. As the solution is exchanged, there will be an increase in the fluorescence intensity until reaching a saturation point, indicating that the lipid solution has filled the chamber.

▲ CRITICAL STEP After the fluorescence intensity in the measurement chamber has reached saturation values, the flow of lipid solution should be stopped to allow for an incubation period.

? TROUBLESHOOTING

(iv) Flow Tris–NaCl buffer into the microfluidic chamber at a flow rate of 50 µl min^{-1} for 10 min to complete the SALB procedure. Under the fluorescence microscope, the

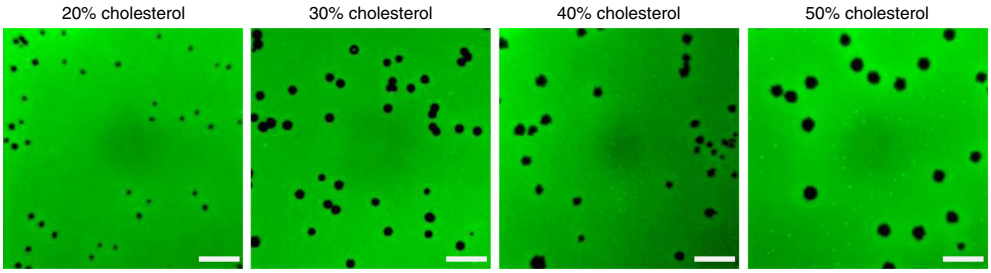

Fig. 5 | Observation of DOPC–cholesterol SLBs on a glass surface by epifluorescence microscopy. The dark spots correspond to cholesterol-enriched regions that are deficient in fluorescently labeled phospholipids. Scale bars, 20 μm. Adapted with permission from ref. [27], American Chemical Society.

fluorescence intensity in the bulk solution should begin to decrease. The focus should be placed on the evolving SLB on the coverslip, where the fluorescence intensity will become uniform across the field of view.

▲ **CRITICAL STEP** It is important to maintain focus on the SLB–silicon oxide interface. A few bright specks, which are typically attributed to lipid aggregates, might form in the SLB vicinity and can serve as reference points for locating the focal plane.

(v) Wash the measurement chamber by flowing Tris–NaCl buffer at a flow rate of at least 100 μl min^{-1} for 10 min. After washing, a uniformly smooth fluorescent image that is not grainy and that is free from dark spots or bright specks should be visible under the fluorescence microscope. For cholesterol-incorporated SLBs, distinct randomly distributed dark spots will be observable; these occur due to fluorophore-poor regions where cholesterol molecules predominate (refer to Fig. 5).

? TROUBLESHOOTING

■ **PAUSE POINT** The SLB-coated coverslip chamber can be stably kept in Tris–NaCl buffer within the microfluidic chamber before further application. It should be used within a few hours for best results.

(vi) Perform FRAP measurement by illuminating the SLB with a high-intensity laser for 5 s and start time-lapse recording for at least 2 min with 2-s intervals.

▲ **CRITICAL STEP** Ensure that the SLB is in the focal plane by keeping the edge of the photobleached spot as sharp as possible. Poor focus may result in inaccurate diffusivity measurements. In addition, the recommended 5-s excitation time and 2-min post bleaching recording time are standard measurement conditions, although optimization might be required, depending on the laser intensity and other instrumental factors.

? TROUBLESHOOTING

(vii) Calculate the diffusivity and mobile fraction of the SLB using the Hankel transform method[73] or another appropriate analysis method. The data fitting can be performed using MATLABwith the Image Processing Toolbox or another suitable software package.

(B) **SLB fabrication with QCM-D monitoring**

(i) After stabilization in Step 4B(iv), restart the measurement and further stabilize the measurement signals at a fixed flow rate of 100 μl min^{-1} for at least another 10 min.

▲ **CRITICAL STEP** Starting with buffer in the measurement chamber as the baseline signal is important to interpreting SLB fabrication quality using the QCM-D technique. It is critical for the frequency and dissipation values to remain stable during this initial step, because they will serve as the baseline values for determining subsequent frequency and energy dissipation shifts. The net frequency and energy dissipation shifts corresponding to SLB formation will be computed relative to the baseline values. If the values start to drift, restart the measurement. Ensure that the tubing settings on the pump correspond to the as-used, three-stop flexible tubing (for pump), e.g., i.d. = 0.76 mm, as recommended in this protocol.

(ii) Introduce IPA into the measurement chamber at a flow rate of 100 μl min^{-1} for 10 min and stabilize the measurement signals. Upon introduction, the frequency (Δf) shift should sharply decrease to ~−250 Hz before stabilizing at ~−100 Hz. The energy dissipation shift (ΔD) should sharply increase to ~100×10^{-6}, before stabilizing at ~40×10^{-6}. These shifts are due to solvent mixing and principally reflect changes in the bulk solution properties.

Table 2 | Reference QCM-D measurement responses after the SALB procedure is completed for DOPC SLBs on different solid supports

Surface	Final Δf (Hz)	Final ΔD ($\times 10^{-6}$)
SiO_2	−26	0.4
Al_2O_3	−38	1.2
Au	−27	0.5
TiO_2	−30	2.0
ITO	−26	0.5
Cr	−26	0.5

Table 3 | Reference QCM-D measurement responses after the SALB procedure is completed for DOPC/cholesterol SLBs on silicon oxide surfaces

Cholesterol fraction (mol%)	Final Δf (Hz)	Final ΔD ($\times 10^{-6}$)
0	−26	0.3
17	−26	0.6
35	−32	1.3
52	−32	1.3

▲ **CRITICAL STEP** Always stop the flow before switching solvents to ensure that no air bubbles are introduced into the measurement chamber. Air bubbles can hinder effective mixing during the solvent-exchange step. The flow rate should be maintained while the signals reach stable values in IPA before proceeding to the next step.

■ **PAUSE POINT** Once the measurement signals have stabilized, the flow can be maintained while lipid solutions are being prepared (see 'Reagent setup' section and Box 1).

(iii) Once the frequency and dissipation values have stabilized, flow 0.5 mg ml^{-1} lipid mixture in IPA into the measurement chamber at a flow rate of 100 µl min^{-1} for at least 10 min until the measurement signals stabilize. The frequency shift is expected to decrease by ~−5 to −7 Hz, while the energy dissipation signal remains stable.

▲ **CRITICAL STEP** The target frequency shift is a general value that is relevant across different surfaces. If the magnitude of the frequency shift is much larger than −7 Hz, then it is possible that the SLB formation process will also involve nucleation of additional lipid structures. If the magnitude of the shift is appreciably smaller than −5 Hz, then it is possible that incomplete SLB formation will occur. The frequency shift associated with lipid adsorption in organic solvent can be adjusted by varying the bulk lipid concentration during the incubation step until the target range is achieved. An important caveat is that the attached lipid during this step is in equilibrium with the bulk lipid[19], and hence the optimal bulk lipid concentration can slightly vary depending on the lipid components in the mixture and the choice of surface.

(iv) Flow Tris–NaCl buffer into the system at a flow rate of 100 µl min^{-1} for 20 min in order to promote SLB formation. During this step, abrupt changes in the frequency and energy dissipation signals will occur initially due to solvent exchange before stabilizing due to SLB formation. Reference values for DOPC SLBs on different surfaces are provided in Table 2 (refs. [19,22,23,25]), and silicon oxide-supported SLBs with different DOPC/cholesterol molar ratios are shown in Table 3 (ref. [29]).

▲ **CRITICAL STEP** Ensure there is no air trapped in the tubing before the solvent-exchange step is performed and make sure to stop the pump flow when exchanging the inlet flow from IPA to aqueous buffer.

? TROUBLESHOOTING

(Optional) Characterization analysis ● Timing ~20–40 min

6 After SLB fabrication is completed, various assays can be performed using the QCM-D measurement technique for SLB characterization (following Step 5B). For surface coverage assessment, follow option A. For lipid fraction evaluation, follow option B. For cholesterol fraction evaluation, follow option C.

(A) **Surface coverage assessment ● Timing ~20 min**

(i) After SLB formation has been completed by following Step 5B, flow 10 μM BSA in Tris–NaCl buffer into the measurement chamber at a flow rate of 100 μl min^{-1} for 10 min.

▲ CRITICAL STEP A control experiment should be performed on an equivalent surface without SLB in order to determine the relative extent of BSA uptake.

▲ CRITICAL STEP Bubbles can easily form in the aqueous solution due to foaming when BSA is initially dissolved. Ensure that the bubbles settle before the experiment and are not introduced into the flow system.

? TROUBLESHOOTING

(ii) Wash the SLB by flowing Tris–NaCl buffer into the measurement chamber at a flow rate of 100 μl min^{-1} for at least another 10 min until the measurement signals stabilize.

▲ CRITICAL STEP The QCM-D measurement responses, especially the Δf shifts, should be recorded after buffer washing for the SLB-coated and bare surfaces. The ratio of the two measurement responses can be used to estimate the SLB fractional surface coverage. The approach is applicable to zwitterionic SLBs, and >90% reduction in BSA uptake is reasonable for a good-quality SLB according to the QCM-D measurement responses.

(B) **Lipid fraction evaluation ● Timing ~40 min**

(i) After the formation of a phosphatidylserine (PS) lipid–containing SLB following Step 5B, exchange the solution to Tris–NaCl–$CaCl_2$ buffer in the measurement chamber.

(ii) Add 5 μg ml^{-1} annexin A5 protein in Tris–NaCl–$CaCl_2$ buffer into the measurement chamber at a flow rate of 100 μl min^{-1} for 30 min.

▲ CRITICAL STEP Annexin A5 binds specifically to PS lipids. Therefore, the PS lipid fraction can be estimated by converting the QCM-D measurement responses into the bound mass of adsorbed protein. Alternatively, the protein can be fluorescently labeled in order to quantify the PS lipid fraction on the basis of a fluorescence intensity readout (follow Step 5A, without fluorescently labeled lipid).

? TROUBLESHOOTING

(iii) Wash the SLB by flowing Tris–NaCl buffer into the measurement chamber at a flow rate of 100 μl min^{-1} for at least another 10 min.

(C) **Cholesterol fraction evaluation ● Timing ~40 min**

(i) After the formation of a cholesterol-containing SLB following Step 5B, add 1 mM MβCD in Tris–NaCl buffer and flow the solution into the measurement chamber at a flow rate of 100 μl min^{-1} until the measurement signals stabilize.

▲ CRITICAL STEP The MβCD solution should be prepared immediately before introduction into the measurement chamber. It is important to wait for the signals to fully stabilize (at least 15–20 min) before determining the final Δf shift. Typically, Δf shifts of ~2–12 Hz will be observed in the presence of 10–50 mol% cholesterol within the SLB, respectively.

? TROUBLESHOOTING

(ii) After the measurement signals have stabilized, the amount of cholesterol mass that is removed can be determined by applying the Sauerbrey equation[98] or equivalent. Likewise, the amount of lipid mass remaining can be determined by the same approach. Thus, by also taking into account the molecular mass values of the different SLB components, the molar ratio of cholesterol in the SLB can be determined by comparing the amount of lipid remaining in the SLB and the amount of cholesterol that was removed.

(Optional) Biofunctionalization ● Timing ~3 h

7 The SLBs can be optionally biofunctionalized for cell culture and biological assay applications. To functionalize SLBs with ECM proteins, follow option A. To incorporate PI for kinase activity monitoring, follow option B.

(A) **Functionalization with ECM proteins** ● Timing ~3 h

(i) After the formation of a DP-NGPE-containing SLB is completed (by following Steps 5B (i)–5B(iv)), flow HEPES–NaCl buffer into the measurement chamber at a flow rate of 50 µl min^{-1} for 10 min.

(ii) Prepare a mixture of 10 mg ml^{-1} EDC–NHS in HEPES–NaCl buffer and flow the solution into the measurement chamber at a flow rate of 50 µl min^{-1} for at least 5 min. Then stop the flow and incubate the system for 1 h to activate the carboxylic acid group of the DP-NGPE lipids before proceeding to the next step.

▲ CRITICAL STEP The EDC–NHS mixture should be prepared immediately before injection.

(iii) Resume the flow with HEPES–NaCl buffer (without EDC–NHS) at a flow rate of 50 µl min^{-1} for 10 min to rinse away excess EDC–NHS molecules from the bulk solution.

(iv) Exchange solutions and flow PBS into the measurement chamber at a flow rate of 50 µl min^{-1} for 10 min.

(v) Add 0.2 mg ml^{-1} of the desired ECM protein in PBS (pH 7.4) and flow the mixture into the measurement chamber at a flow rate of 50 µl min^{-1} for ~10 min. Then stop the flow and incubate the system for 2 h before proceeding to the next step.

(vi) Resume flow with PBS (without protein) at a rate of 50 µl min^{-1} for 20 min to remove weakly bound proteins.

■ PAUSE POINT The ECM protein–functionalized SLBs can be kept in aqueous buffer until further experimentation and should preferably be used within a few hours.

(B) **Incorporation of PI for kinase activity monitoring** ● Timing ~3 h

(i) Upon the successful formation of 10 wt% PI lipid–containing SLB, wash the bilayer by flowing Tris–NaCl buffer into the measurement chamber at a flow rate of 50 µl min^{-1} for at least another 10 min. The following steps describe operation with QCM-D monitoring, although Step 7B(ii–v) can be performed in a conventional microfluidic flow system in conjunction with other measurement options as well.

■ PAUSE POINT The PI lipid–containing SLBs can be stored in aqueous buffer and should preferably be used within a few hours.

(ii) For characterizing the PI4Kβ enzyme, raise the chamber temperature to 30 °C while maintaining the flow of Tris–NaCl buffer. Wait for the signal to stabilize.

▲ CRITICAL STEP Increasing the temperature from 25 to 30 °C will lead to slight changes in the frequency and energy dissipation signals due to changes in the bulk solution properties. Ensure that the frequency and energy dissipation signals have fully stabilized before proceeding to the next step.

? TROUBLESHOOTING

(iii) Flow kinase buffer into the measurement chamber at a flow rate of 50 µl min^{-1} for 10 min.

(iv) Add 2.5 nM PI4Kβ in kinase buffer at a flow rate of 50 µl min^{-1} for ~90 min. If active, the enzyme will convert PI in the SLB into PI4P.

(v) Flow Tris–NaCl buffer into the measurement chamber at a flow rate of 50 µl min^{-1} for 20 min and lower the temperature to 25 °C. Stabilize the signal.

▲ CRITICAL STEP Ensure that buffer exchange has been completed and the signals have stabilized before lowering the temperature. Ensure that the frequency and energy dissipation signals have completely stabilized before proceeding to the next step.

? TROUBLESHOOTING

(vi) To verify the generation of PI4P, add 5 µg ml^{-1} anti-PI4P IgM antibody in Tris–NaCl buffer into the measurement chamber at a flow rate of 50 µl min^{-1} and stabilize the signal.

? TROUBLESHOOTING

(vii) To calculate the conversion yield of PI into PI4P, perform an identical control experiment using 10 wt% PI4P instead of 10 wt% PI in Step 7B(i) and then perform Step 7B(vi). Using the QSense Dfind software package, apply the Voigt–Voinova model to both data sets in order to estimate the number of antibodies bound to the SLBs. The ratio between the two values represents the conversion yield, which will be ~80–90% if the enzyme is working well.

Troubleshooting

Troubleshooting advice can be found in Table 4.

Table 4 | Troubleshooting table

Step	Problem	Possible reason	Solution
4A(i)	Buffer leaks from the microfluidic chamber	The adhesion between the microfluidic chip and the glass coverslip is poor or uneven	Apply additional force by pressing the glass coverslip against the microfluidic chip to avoid air bubbles Repeat the experiment with a new microfluidic chip. When attaching the glass coverslip to the microfluidic chip, ensure that the pressing is done on a flat surface
		The glass coverslip is cracked	Repeat the experiment with a new glass coverslip and microfluidic chip set
4A(vi)	Generation of air bubbles between the elbow connector and the chamber	The inlet/outlet tube or the chamber is not fully filled with buffer	Unplug the connector, run the flow in the reverse direction, and check that the connectors are fully filled Fill the chamber with buffer
4A(vii)	The buffer does not exit the outlet tubing, or the solution flow is weak and irregular	The microfluidic chip is not assembled correctly	See troubleshooting advice for Step 4A(i)
		The elbow connector is not fixed well or is damaged	Gently push down the elbow connector Change the elbow connector
		The section of the three-stop flexible tubing attached to the pump roller-head is fatigued	Switch to a fresh section of the flexible tubing Replace the flexible tubing
		There is residual fluid or contaminants in the Teflon tubing	Replace the Teflon tubing
		The tubing diameter selected in the pump setting is incorrect	Correct the tubing diameter in the pump setting
4B(iii)	The buffer does not exit the outlet tubing	Air bubbles are generated in the flow module or tubes	Briefly switch the solution flow to a higher flow rate to clear the air bubble via the outlet Reverse the solution flow to clear the air bubble via the inlet
		The sensor chip is not mounted properly and is broken	Open the chamber and check the sensor chip condition. Ensure that the sensor chip is mounted properly. If broken, change to a new sensor chip and repeat from Step 4B(i)
	The solution flow is weak and irregular	The section of the three-stop flexible tubing attached to the pump roller-head is fatigued	Switch to a fresh section of the flexible tubing Replace the flexible tubing
		There is residual fluid or contaminants in the Teflon tubing	Replace the Teflon tubing
		The tubing diameter selected in the pump setting is incorrect	Correct the tubing diameter in the pump setting
5A(i)	Generation of air bubbles in the inlet tube	Inefficient mixing between IPA and buffer	Reverse the flow direction to remove air bubbles Reduce the flow speed
5A(iii)	The sample shows weak or no fluorescence	The image is out of focus	Carefully adjust the focus over the entire depth until the solid–liquid interface falls within the focal plane Repeat with a fresh lipid stock. Ensure that the fluorescent lipid stock is not more than 3 months old
5A(v)	Too many defects are observed as dark spots Bright fluorescent specks are visible	The glass coverslip is contaminated or not properly cleaned Other lipid phases (e.g., micelles, vesicles) remain adsorbed on the surface in trace amounts	Extensively clean the glass coverslip and repeat the experiment Allow more time for the buffer to flow during the washing step Increase the buffer flow rate during the washing step
5A(vi)	The fluorescence intensity does not decrease to <30% of its original intensity	The photobleaching duration or laser power is not sufficient	Increase the photobleaching duration or the laser power
	Appreciable fluorescence recovery takes more than 3 min	The lipid composition might affect membrane fluidity	Increase the duration of image recording and decrease the imaging time interval to avoid excessive photobleaching
5B(iv)	The Δf shift remains unchanged	The solvent does not reach the substrate because of air bubble formation or leakage	Check that there are no air bubbles or leakage before the buffer reaches the measurement chamber Ensure that the tubing connections are secure

Table continued

Table 4 (continued)

Step	Problem	Possible reason	Solution
	The Δf value does not stabilize at the desired value	Air bubbles are generated inside the chamber	Switch back to aqueous buffer and repeat the experiment from the SDS washing step
	The Δf shift stabilized at a value that is lower than expected	Lipid molecules have become degraded in IPA	Repeat the experiment with a fresh lipid sample and make sure to avoid strong vortexing
6A(i)	BSA adsorption is higher than expected	Formation of an incomplete bilayer with high defect density occurred	Ensure that the concentration of lipid dissolved in organic solvent is correct Repeat the experiment from the washing step
		Adsorption of BSA aggregates on the substrate surface occurred	BSA molecules are aggregated due to prolonged storage. Repeat the experiment with a fresh BSA solution. Ensure that the BSA is fully dissolved in Tris–NaCl buffer
6B(ii)	There is no additional Δf shift when annexin A5 is added	DOPS lipids are not present in the SLB	Repeat the experiment with fresh DOPS lipids. Ensure that the lipid powder or lipid stock in chloroform is not expired
			Repeat the experiment, ensuring that the lipids are dispersed well in the organic solvent
		Aggregates of annexin A5 are formed in the solution	Repeat with a freshly prepared annexin A5 solution. If necessary, use a new batch of annexin A5
6C(i)	There is no additional Δf shift	Cholesterol is not present in the SLB	Check the concentration of cholesterol in the lipid–cholesterol mixture and repeat the experiment. If necessary, increase the cholesterol fraction Repeat the experiment, ensuring that the cholesterol is mixed well with the lipids in the organic solvent Repeat the experiment using a new batch of cholesterol
		Aggregates of MβCD formed in the solution	Repeat with a freshly prepared MβCD solution. If necessary, use a new batch of MβCD
7B(ii)	The signal does not stabilize after the temperature is increased	There is air bubble formation in the flow module or tubes	Briefly switch the solution flow to a higher flow rate to clear potential air bubbles
			Ensure that the buffer is degassed, as dissolved gas can be released during heating to form air bubbles
		The sensor may experience a transient 'temperature shock'	Reset the temperature to 25 °C and repeat the step. Ensure that the buffer is equilibrated to room temperature before introduction into the measurement chamber
7B(v)	The signal does not stabilize after the temperature is lowered	The sensor may experience a transient 'temperature shock'	Reset the temperature to 30 °C and repeat the step. Ensure that the buffer is equilibrated to room temperature before introduction into the measurement chamber
7B(vi)	There is no change in the measurement signals	The PI in the SLB does not become phosphorylated to PI4P	Repeat the phosphorylation step using a new batch of PI4Kβ kinase Repeat the phosphorylation step using a freshly prepared kinase buffer
		There is poor recognition of PI4P by the anti-PI4P antibody	Repeat using a new batch of anti-PI4P IgM antibody
Box 1, step A(i)	The lipids do not fully dissolve in the solvent, resulting in a turbid solution	Charged lipids do not dissolve well in IPA	Use ethanol as the organic solvent for charged lipids. Ensure that only absolute ethanol is used; ethanol with lower purity may not sufficiently dissolve lipids
		The heating temperature is not high enough to improve solubility	Ensure that the heating temperature is at least ~50 °C. If necessary, increase the temperature to ~60 °C

Timing

Steps 1–4, microfluidic chamber setup: ~15 min
Step 5, SLB fabrication: ~30 min
Step 6, (optional) characterization analysis: ~20–40 min
Step 7, (optional) biofunctionalization: ~3 h
Box 1, lipid solution preparation: ~15 min

Anticipated results

The SALB procedure was developed in order to make SLB fabrication a mainstream process that can be adopted by scientific researchers from different disciplines. To achieve this goal, the basic procedure was designed so that users can readily acquire the necessary skills in a short period of time. After a few rounds of practice, it is anticipated that most users will be able to consistently form SLBs using the SALB procedure. Particular skills that must be emphasized include proper handling of lipids and the ability to assemble commercially available microfluidics (Fig. 4). With these skills and experience in hand, users will be able to quickly grasp the SALB procedure and use it to fabricate SLBs for a wide range of applications. In such cases, one might not necessarily characterize the SLB formation process every time but rather focus on using validated SLB platforms for downstream bioanalytical assays, as demonstrated herein with the examples of ECM biofunctionalization and kinase activity monitoring assays.

In addition, there is an excellent opportunity to utilize the SALB procedure for fundamental biophysical studies among more experienced users. Typically, it is difficult to form SLBs on various material supports such as gold and titanium oxide, and the SALB procedure provides an effective strategy for forming SLBs on these previously intractable material supports. As discussed above, it has proven useful to compare the effectiveness of the conventional vesicle fusion method and that of the SALB method in order to gain insight into lipid–substrate interactions on different material supports. Recent evidence points to vesicle fusion succeeding on surfaces for which there are strong lipid–substrate interactions and low degrees of surface hydration, whereas the method does not work when there are relatively weaker (but still attractive) lipid–substrate interactions and high degrees of surface hydration. In marked contrast, the SALB procedure is able to form SLBs in both cases, demonstrating its broad versatility. For example, QCM-D data for successful SLB formation via the SALB procedure on different surfaces, including silicon oxide, gold, titanium oxide, and aluminum oxide, are presented in Fig. 6; these data demonstrate that the fabricated SLBs remain stably bound in all cases for at least 1 d. It should be emphasized that there are attractive lipid–substrate interactions in all these cases, and that is a prerequisite for successful SLB formation (see Supplementary Fig. 2 for pH-dependent cases in which SLB formation does not occur because of repulsive lipid–substrate interactions). Although lipid–substrate interactions are typically classified as 'weak' on substrates such as gold and titanium oxide, such statements are primarily relevant in the context of the vesicle fusion method. In that case, the lipid–substrate interactions on gold and titanium oxide surfaces are attractive enough to support vesicle adsorption but are often insufficiently strong to induce subsequent rupture of adsorbed vesicles. In this respect, the SALB method is advantageous because it requires only a minimum threshold of attractive lipid–substrate interactions and there is no high-energy requirement for vesicle rupture, which is typically the rate-limiting step in the vesicle fusion method.

Interestingly, however, the measurement responses associated with SLBs formed on different material supports by using the SALB procedure are not always identical, and it is important to note that these deviations are oftentimes due to variations in lipid–substrate interactions rather than incomplete bilayer formation. Although the lipid–substrate interactions are attractive in all cases in which SLBs are formed, there is a spectrum of interaction strengths. With greater interaction

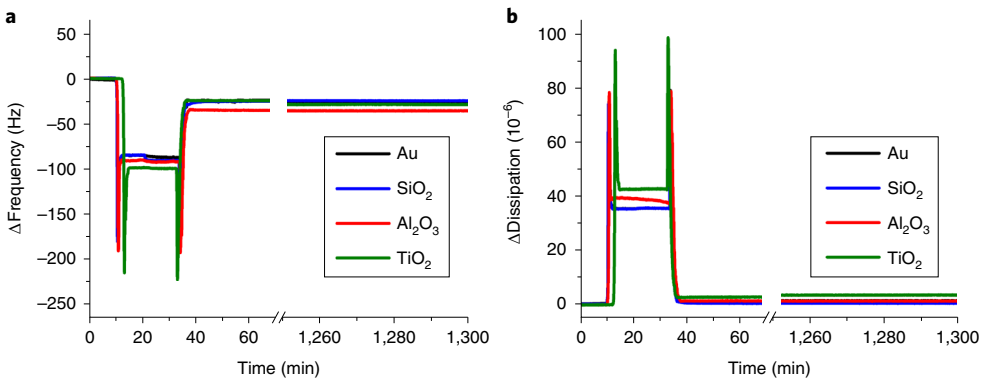

Fig. 6 | QCM-D of SLB formation on different substrates. a,**b**, Frequency (**a**) and energy dissipation (**b**) shifts tracking SLB formation on different substrates, followed by overnight incubation under continuous buffer flow.

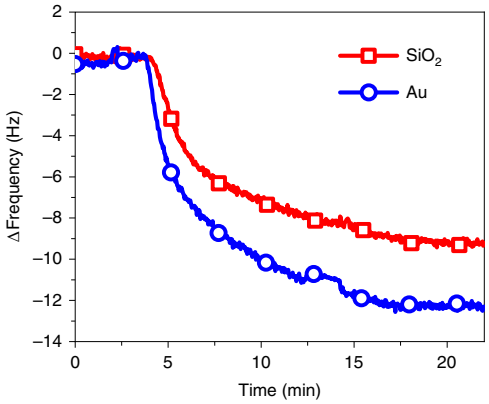

Fig. 7 | QCM-D of streptavidin binding to functionalized SLBs. QCM-D characterization of streptavidin binding to 5 mol% biotinylated lipid-functionalized SLBs on silicon oxide and gold surfaces.

strength, there is tighter coupling of the SLB to the underlying solid support and hence a thinner hydration layer. This results in less-coupled hydration mass because the hydration layer is smaller. As presented in Table 2, the anticipated QCM-D responses for a complete SLB on different material supports vary, and the differences are due to variations in the amount of coupled solvent in the hydration layer separating the SLB from the underlying material support. As a general trend, if there is more hydration mass, then the QCM-D measurement responses are greater. In addition, if an SLB is more strongly coupled to a solid support, then there can be lower lateral lipid diffusivity as well[88]. Practically, different lipid–substrate interactions on various surfaces can result in slightly different lipid compositions for multi-component SLB platforms. A QCM-D measurement example of streptavidin binding to 5 mol% biotinylated lipid-functionalized SLBs on silicon oxide and gold surfaces is shown in Fig. 7, where the degree of streptavidin binding is evaluated (larger frequency shift corresponds to more protein binding).

Similar considerations hold for other functional properties of SLBs, including the effects of sterols on membrane organization. For example, depending on the molar fraction of cholesterol in an SLB, the lipid bilayer packing will change, and hence the QCM-D responses will vary as presented in Table 3. Such properties can be further investigated by fluorescence microscopy, and the images in Fig. 5 show how cholesterol can affect the phase properties of SLBs. More complex structural arrangements are envisioned with diverse lipid compositions, especially when including phospholipids with different phase properties, sterols, and other lipids such as sphingomyelin. Indeed, in recent years, there have been extensive efforts aimed at preparing SLBs from natural cell membranes[99–106], and exploring the suitability of the SALB method to work with these compositions would open the door to new research opportunities. Although we have demonstrated the successful conjugation of membrane-associated proteins to SLBs prepared via the SALB method, another potential advantage of the SALB method might be the ability to incorporate membrane proteins during the fabrication step itself. Past findings show that proteins in organic solvents do not undergo denaturation[107], and therefore we envision that lipid and protein mixtures might be deposited in a water-miscible organic solvent as part of the SALB procedure and yield membrane protein-embedded SLB platforms.

The aforementioned measurement examples in this protocol involve QCM-D and fluorescence microscopy experiments, and there are many more possibilities, depending on the application needs. Other measurement options include label-free optical biosensors (e.g., surface plasmon resonance, localized surface plasmon resonance, ellipsometry, reflectometry), atomic force microscopy, neutron reflectometry, and electrochemical impedance spectroscopy. In all cases, it is important to gain practical experience with data interpretation, and successful implementation of the protocol must be accompanied by a nuanced understanding of the measurement responses that take into account the physicochemical properties of the SLB system under consideration along with the physical principles behind the selected measurement techniques. Oftentimes, it is advisable to use multiple surface-sensitive measurement techniques to characterize SLB properties, especially at the beginning stages of a project, in order to validate an optimized SALB procedure. Such issues are particularly important when working with complex lipid compositions in which multiple phase states can occur and the SLB may not exhibit homogeneous properties. Thus, we recommend that careful selection of the appropriate measurement techniques be decided on the basis of the experimental objective and

membrane features. Overall, the SALB procedure opens the door to broadly understanding the fundamental nature of SLBs on material supports. In turn, these insights provide an avenue to engineering improved SLB platforms for various applications.

Looking forward, the SALB procedure demonstrates excellent potential for increasing the use of SLB platforms in different scientific fields. It is the first SLB fabrication method that is truly versatile and that can be simply implemented by novice and experienced users alike. Given these advantages, there is ample opportunity to explore SLBs as cell membrane models and as biocompatible coatings among numerous other application possibilities.

Reporting Summary

Further information on research design is available in the Nature Research Reporting Summary linked to this article.

Data availability

The datasets generated during and/or analyzed during the current study are available from the corresponding authors upon reasonable request.

References

1. Richter, R. P., Bérat, R. & Brisson, A. R. Formation of solid-supported lipid bilayers: an integrated view. *Langmuir* **22**, 3497–3505 (2006).
2. Castellana, E. T. & Cremer, P. S. Solid supported lipid bilayers: From biophysical studies to sensor design. *Surface Sci. Rep.* **61**, 429–444 (2006).
3. Chan, Y.-H. M. & Boxer, S. G. Model membrane systems and their applications. *Curr. Opin. Chem. Biol.* **11**, 581–587 (2007).
4. Reimhult, E. & Kumar, K. Membrane biosensor platforms using nano-and microporous supports. *Trends Biotechnol.* **26**, 82–89 (2008).
5. Im, H., Wittenberg, N. J., Lesuffleur, A., Lindquist, N. C. & Oh, S.-H. Membrane protein biosensing with plasmonic nanopore arrays and pore-spanning lipid membranes. *Chem. Sci.* **1**, 688–696 (2010).
6. Yang, T., Jung, S., Mao, H. & Cremer, P. S. Fabrication of phospholipid bilayer-coated microchannels for on-chip immunoassays. *Anal. Chem.* **73**, 165–169 (2001).
7. Junesch, J. et al. Location-specific nanoplasmonic sensing of biomolecular binding to lipid membranes with negative curvature. *Nanoscale* **7**, 15080–15085 (2015).
8. Mingeot-Leclercq, M.-P., Deleu, M., Brasseur, R. & Dufrêne, Y. F. Atomic force microscopy of supported lipid bilayers. *Nat. Protoc.* **3**, 1654 (2008).
9. Cho, N.-J., Frank, C. W., Kasemo, B. & Höök, F. Quartz crystal microbalance with dissipation monitoring of supported lipid bilayers on various substrates. *Nat. Protoc.* **5**, 1096–1106 (2010).
10. Lee, T.-H., Hirst, D. J., Kulkarni, K., Del Borgo, M. P. & Aguilar, M.-I. Exploring molecular-biomembrane interactions with surface plasmon resonance and dual polarization interferometry technology: expanding the spotlight onto biomembrane structure. *Chem. Rev.* **118**, 5392–5487 (2018).
11. Höök, F. et al. Supported lipid bilayers, tethered lipid vesicles, and vesicle fusion investigated using gravimetric, plasmonic, and microscopy techniques. *Biointerphases* **3**, FA108–FA116 (2008).
12. Mashaghi, A. et al. Label-free characterization of biomembranes: from structure to dynamics. *Chem. Soc. Rev.* **43**, 887–900 (2014).
13. Limaj, O. et al. Infrared plasmonic biosensor for real-time and label-free monitoring of lipid membranes. *Nano Lett.* **16**, 1502–1508 (2016).
14. Tabaei, S. R., Choi, J.-H., Haw Zan, G., Zhdanov, V. P. & Cho, N.-J. Solvent-assisted lipid bilayer formation on silicon dioxide and gold. *Langmuir* **30**, 10363–10373 (2014).
15. Deshpande, S. & Dekker, C. On-chip microfluidic production of cell-sized liposomes. *Nat. Protoc.* **13**, 856 (2018).
16. Doktorova, M. et al. Preparation of asymmetric phospholipid vesicles for use as cell membrane models. *Nat. Protoc.* **13**, 2086 (2018).
17. Szoka, F. & Papahadjopoulos, D. Procedure for preparation of liposomes with large internal aqueous space and high capture by reverse-phase evaporation. *Proc. Natl Acad. Sci.* **75**, 4194–4198 (1978).
18. Hohner, A. O., David, M. P. C. & Rädler, J. O. Controlled solvent-exchange deposition of phospholipid membranes onto solid surfaces. *Biointerphases* **5**, 1–8 (2010).
19. Tabaei, S. R., Jackman, J. A., Kim, S.-O., Zhdanov, V. P. & Cho, N.-J. Solvent-assisted lipid self-assembly at hydrophilic surfaces: factors influencing the formation of supported membranes. *Langmuir* **31**, 3125–3134 (2015).
20. Kim, M. C., Gillissen, J. J., Tabaei, S. R., Zhdanov, V. P. & Cho, N.-J. Spatiotemporal dynamics of solvent-assisted lipid bilayer formation. *Phys. Chem. Chem. Phys.* **17**, 31145–31151 (2015).
21. Gillissen, J. J., Tabaei, S. R. & Cho, N.-J. A phenomenological model of the solvent-assisted lipid bilayer formation method. *Phys. Chem. Chem. Phys.* **18**, 24157–24163 (2016).

22. Jackman, J. A., Tabaei, S. R., Zhao, Z., Yorulmaz, S. & Cho, N.-J. Self-assembly formation of lipid bilayer coatings on bare aluminum oxide: overcoming the force of interfacial water. *ACS Appl. Mater. Interfaces* **7**, 959–968 (2014).
23. Tabaei, S. R., Ng, W. B., Cho, S.-J. & Cho, N.-J. Controlling the formation of phospholipid monolayer, bilayer, and intact vesicle layer on graphene. *ACS Appl. Mater. Interfaces* **8**, 11875–11880 (2016).
24. Losada-Pérez, P., Polat, O., Parikh, A. N., Seker, E. & Renner, F. U. Engineering the interface between lipid membranes and nanoporous gold: a study by quartz crystal microbalance with dissipation monitoring. *Biointerphases* **13**, 011002 (2018).
25. Tabaei, S. R., Vafaei, S. & Cho, N.-J. Fabrication of charged membranes by the solvent-assisted lipid bilayer (SALB) formation method on SiO_2 and Al_2O_3. *Phys. Chem. Chem. Phys.* **17**, 11546–11552 (2015).
26. Tabaei, S. R. et al. Multistep compositional remodeling of supported lipid membranes by interfacially active phosphatidylinositol kinases. *Anal. Chem.* **88**, 5042–5045 (2016).
27. Tabaei, S. R. et al. Formation of cholesterol-rich supported membranes using solvent-assisted lipid self-assembly. *Langmuir* **30**, 13345–13352 (2014).
28. Tabaei, S. R., Jackman, J. A., Liedberg, B., Parikh, A. N. & Cho, N.-J. Observation of stripe superstructure in the β-two-phase coexistence region of cholesterol–phospholipid mixtures in supported membranes. *J. Am. Chem. Soc.* **136**, 16962–16965 (2014).
29. Kawakami, L. M. et al. Understanding how sterols regulate membrane remodeling in supported lipid bilayers. *Langmuir* **33**, 14756–14765 (2017).
30. Sundh, M., Svedhem, S. & Sutherland, D. S. Influence of phase separating lipids on supported lipid bilayer formation at SiO_2 surfaces. *Phys. Chem. Chem. Phys.* **12**, 453–460 (2010).
31. Crane, J. M. & Tamm, L. K. Role of cholesterol in the formation and nature of lipid rafts in planar and spherical model membranes. *Biophys. J.* **86**, 2965–2979 (2004).
32. Stottrup, B. L., Veatch, S. L. & Keller, S. L. Nonequilibrium behavior in supported lipid membranes containing cholesterol. *Biophys. J.* **86**, 2942–2950 (2004).
33. Ziblat, R., Kjaer, K., Leiserowitz, L. & Addadi, L. Structure of cholesterol/lipid ordered domains in monolayers and single hydrated bilayers. *Angew. Chem. Int. Ed. Engl.* **48**, 8958–8961 (2009).
34. Lee, T.-H., Hirst, D. J. & Aguilar, M.-I. New insights into the molecular mechanisms of biomembrane structural changes and interactions by optical biosensor technology. *Biochim. Biophys. Acta* **1848**, 1868–1885 (2015).
35. Czogalla, A., Grzybek, M., Jones, W. & Coskun, Ü. Validity and applicability of membrane model systems for studying interactions of peripheral membrane proteins with lipids. *Biochim. Biophys. Acta* **1841**, 1049–1059 (2014).
36. Wittenberg, N. J. et al. High-affinity binding of remyelinating natural autoantibodies to myelin-mimicking lipid bilayers revealed by nanohole surface plasmon resonance. *Anal. Chem.* **84**, 6031–6039 (2012).
37. Rascol, E., Devoisselle, J.-M. & Chopineau, J. The relevance of membrane models to understand nanoparticles–cell membrane interactions. *Nanoscale* **8**, 4780–4798 (2016).
38. Costello, D. A., Villareal, V. A. & Yang, P. L. Desmosterol increases lipid bilayer fluidity during hepatitis C virus infection. *ACS Infect. Dis.* **2**, 852–862 (2016).
39. Naumann, R. et al. Incorporation of membrane proteins in solid-supported lipid layers. *Angew. Chem. Int. Ed. Engl.* **34**, 2056–2058 (1995).
40. Robelek, R. et al. Incorporation of in vitro synthesized GPCR into a tethered artificial lipid membrane system. *Angew. Chem. Int. Ed. Engl.* **46**, 605–608 (2007).
41. Chadli, M. et al. New tethered phospholipid bilayers integrating functional G-protein-coupled receptor membrane proteins. *Langmuir* **33**, 10385–10401 (2017).
42. Chadli, M. et al. A new functional membrane protein microarray based on tethered phospholipid bilayers. *Analyst* **143**, 2165–2173 (2018).
43. Boxer, S. G. Molecular transport and organization in supported lipid membranes. *Curr. Opin. Chem. Biol.* **4**, 704–709 (2000).
44. Su, X. et al. Phase separation of signaling molecules promotes T cell receptor signal transduction. *Science* **352**, 595–599 (2016).
45. Van Oudenaarden, A. & Boxer, S. G. Brownian ratchets: molecular separations in lipid bilayers supported on patterned arrays. *Science* **285**, 1046–1048 (1999).
46. Bally, M. et al. Liposome and lipid bilayer arrays towards biosensing applications. *Small* **6**, 2481–2497 (2010).
47. Yusko, E. C. et al. Controlling protein translocation through nanopores with bio-inspired fluid walls. *Nat. Nanotechnol.* **6**, 253 (2011).
48. Schiller, S. M., Naumann, R., Lovejoy, K., Kunz, H. & Knoll, W. Archaea analogue thiolipids for tethered bilayer lipid membranes on ultrasmooth gold surfaces. *Angew. Chem. Int. Ed. Engl.* **42**, 208–211 (2003).
49. Naumann, R. et al. Tethered lipid bilayers on ultraflat gold surfaces. *Langmuir* **19**, 5435–5443 (2003).
50. Keizer, H. M. et al. Functional ion channels in tethered bilayer membranes—implications for biosensors. *ChemBioChem* **8**, 1246–1250 (2007).
51. Wiegand, G., Arribas-Layton, N., Hillebrandt, H., Sackmann, E. & Wagner, P. Electrical properties of supported lipid bilayer membranes. *J. Phys. Chem. B* **106**, 4245–4254 (2002).
52. Jackman, A. J., Knoll, W. & Cho, N.-J. Biotechnology applications of tethered lipid bilayer membranes. *Materials* **5**, 2637–2657 (2012).

53. Andersson, J., Köper, I. & Knoll, W. Tethered membrane architectures—design and applications. *Front. Mater.* **5**, 55 (2018).
54. De Leo, V. et al. Liposome-modified titanium surface: a strategy to locally deliver bioactive molecules. *Colloids Surf. B Biointerfaces* **158**, 387–396 (2017).
55. Glasmästar, K., Larsson, C., Höök, F. & Kasemo, B. Protein adsorption on supported phospholipid bilayers. *J. Colloid Interface Sci.* **246**, 40–47 (2002).
56. Andersson, A. S., Glasmästar, K., Sutherland, D., Lidberg, U. & Kasemo, B. Cell adhesion on supported lipid bilayers. *J. Biomed. Mater. Res. A* **64**, 622–629 (2003).
57. van Weerd, J., Karperien, M. & Jonkheijm, P. Supported lipid bilayers for the generation of dynamic cell–material interfaces. *Adv. Healthc. Mater.* **4**, 2743–2779 (2015).
58. Koçer, G. & Jonkheijm, P. Guiding hMSC adhesion and differentiation on supported lipid bilayers. *Adv. Healthc. Mater.* **6**, 1600862 (2017).
59. Nair, P. M., Salaita, K., Petit, R. S. & Groves, J. T. Using patterned supported lipid membranes to investigate the role of receptor organization in intercellular signaling. *Nat. Protoc.* **6**, 523 (2011).
60. Glazier, R. & Salaita, K. Supported lipid bilayer platforms to probe cell mechanobiology. *Biochim. Biophys. Acta* **1859**, 1465–1482 (2017).
61. Koçer, G. & Jonkheijm, P. About chemical strategies to fabricate cell-instructive biointerfaces with static and dynamic complexity. *Adv. Healthc. Mater.* **7**, 1701192 (2018).
62. Svedhem, S. et al. In situ peptide-modified supported lipid bilayers for controlled cell attachment. *Langmuir* **19**, 6730–6736 (2003).
63. Huang, C.-J. et al. Type I collagen-functionalized supported lipid bilayer as a cell culture platform. *Biomacromolecules* **11**, 1231–1240 (2010).
64. Yorulmaz Avsar, S. et al. Immobilization strategies for functional complement convertase assembly at lipid membrane interfaces. *Langmuir* **33**, 7332–7342 (2017).
65. Wu, J.-C. et al. Antibody conjugated supported lipid bilayer for capturing and purification of viable tumor cells in blood for subsequent cell culture. *Biomaterials* **34**, 5191–5199 (2013).
66. Chen, J.-Y. et al. Sensitive and specific biomimetic lipid coated microfluidics to isolate viable circulating tumor cells and microemboli for cancer detection. *PLoS One* **11**, e0149633 (2016).
67. Vafaei, S., Tabaei, S. R., Biswas, K. H., Groves, J. T. & Cho, N. J. Dynamic cellular interactions with extracellular matrix triggered by biomechanical tuning of low-rigidity, supported lipid membranes. *Adv. Healthc. Mater.* **6**, 1700243 (2017).
68. Kubalek, E. W., Le Grice, S. F. J. & Brown, P. O. Two-dimensional crystallization of histidine-tagged, HIV-1 reverse transcriptase promoted by a novel nickel-chelating lipid. *J. Struct. Biol.* **113**, 117–123 (1994).
69. Chikh, G. G., Li, W. M., Schutze-Redelmeier, M.-P., Meunier, J.-C. & Bally, M. B. Attaching histidine-tagged peptides and proteins to lipid-based carriers through use of metal-ion-chelating lipids. *Biochim. Biophys. Acta* **1567**, 204–212 (2002).
70. Lata, S., Gavutis, M. & Piehler, J. Monitoring the dynamics of ligand–receptor complexes on model membranes. *J. Am. Chem. Soc.* **128**, 6–7 (2006).
71. Nye, J. A. & Groves, J. T. Kinetic control of histidine-tagged protein surface density on supported lipid bilayers. *Langmuir* **24**, 4145–4149 (2008).
72. Galush, W. J. et al. A nanocube plasmonic sensor for molecular binding on membrane surfaces. *Nano Lett.* **9**, 2077–2082 (2009).
73. Busch, D. J. et al. Intrinsically disordered proteins drive membrane curvature. *Nat. Commun.* **6**, 7875 (2015).
74. van der Meulen, S. A. J., Dubacheva, G. V., Dogterom, M., Richter, R. P. & Leunissen, M. E. Quartz crystal microbalance with dissipation monitoring and spectroscopic ellipsometry measurements of the phospholipid bilayer anchoring stability and kinetics of hydrophobically modified DNA oligonucleotides. *Langmuir* **30**, 6525–6533 (2014).
75. Dubacheva, G. V. et al. Controlling multivalent binding through surface chemistry: model study on streptavidin. *J. Am. Chem. Soc.* **139**, 4157–4167 (2017).
76. Tamm, L. K. & McConnell, H. M. Supported phospholipid bilayers. *Biophys. J.* **47**, 105–113 (1985).
77. Girard-Egrot, A. P. & Blum, L. J. Langmuir-Blodgett technique for synthesis of biomimetic lipid membranes. in *Nanobiotechnology of Biomimetic Membranes* (ed. Martin, D. K.) 23–74 (Springer, 2007).
78. Hardy, G. J., Nayak, R. & Zauscher, S. Model cell membranes: techniques to form complex biomimetic supported lipid bilayers via vesicle fusion. *Curr. Opin. Colloid Interface Sci.* **18**, 448–458 (2013).
79. Keller, C. & Kasemo, B. Surface specific kinetics of lipid vesicle adsorption measured with a quartz crystal microbalance. *Biophys. J.* **75**, 1397–1402 (1998).
80. Keller, C., Glasmästar, K., Zhdanov, V. & Kasemo, B. Formation of supported membranes from vesicles. *Phys. Rev. Lett.* **84**, 5443 (2000).
81. Cremer, P. S. & Boxer, S. G. Formation and spreading of lipid bilayers on planar glass supports. *J. Phys. Chem. B* **103**, 2554–2559 (1999).
82. Biswas, K. H., Jackman, J. A., Park, J. H., Groves, J. T. & Cho, N.-J. Interfacial forces dictate the pathway of phospholipid vesicle adsorption onto silicon dioxide surfaces. *Langmuir* **34**, 1775–1782 (2018).
83. Sackmann, E. Supported membranes: scientific and practical applications. *Science* **271**, 43–48 (1996).

84. Zwang, T. J., Fletcher, W. R., Lane, T. J. & Johal, M. S. Quantification of the layer of hydration of a supported lipid bilayer. *Langmuir* **26**, 4598–4601 (2010).
85. Reimhult, E., Höök, F. & Kasemo, B. Intact vesicle adsorption and supported biomembrane formation from vesicles in solution: influence of surface chemistry, vesicle size, temperature, and osmotic pressure. *Langmuir* **19**, 1681–1691 (2003).
86. Gracià, R. S., Bezlyepkina, N., Knorr, R. L., Lipowsky, R. & Dimova, R. Effect of cholesterol on the rigidity of saturated and unsaturated membranes: fluctuation and electrodeformation analysis of giant vesicles. *Soft Matter* **6**, 1472–1482 (2010).
87. McLaughlin, S. & Murray, D. Plasma membrane phosphoinositide organization by protein electrostatics. *Nature* **438**, 605 (2005).
88. Mager, M. D., Almquist, B. & Melosh, N. A. Formation and characterization of fluid lipid bilayers on alumina. *Langmuir* **24**, 12734–12737 (2008).
89. Mager, M. D. & Melosh, N. A. Lipid bilayer deposition and patterning via air bubble collapse. *Langmuir* **23**, 9369–9377 (2007).
90. Hirtz, M., Oikonomou, A., Georgiou, T., Fuchs, H. & Vijayaraghavan, A. Multiplexed biomimetic lipid membranes on graphene by dip-pen nanolithography. *Nat. Commun.* **4**, 2591 (2013).
91. Lenhert, S., Sun, P., Wang, Y., Fuchs, H. & Mirkin, C. A. Massively parallel dip-pen nanolithography of heterogeneous supported phospholipid multilayer patterns. *Small* **3**, 71–75 (2007).
92. Mennicke, U. & Salditt, T. Preparation of solid-supported lipid bilayers by spin-coating. *Langmuir* **18**, 8172–8177 (2002).
93. Dols-Perez, A., Fumagalli, L., Simonsen, A. C. & Gomila, G. Ultrathin spin-coated dioleoylphosphatidylcholine lipid layers in dry conditions: a combined atomic force microscopy and nanomechanical study. *Langmuir* **27**, 13165–13172 (2011).
94. Dols-Perez, A., Fumagalli, L. & Gomila, G. Structural and nanomechanical effects of cholesterol in binary and ternary spin-coated single lipid bilayers in dry conditions. *Colloids Surf. B Biointerfaces* **116**, 295–302 (2014).
95. Raedler, J., Strey, H. & Sackmann, E. Phenomenology and kinetics of lipid bilayer spreading on hydrophilic surfaces. *Langmuir* **11**, 4539–4548 (1995).
96. Nissen, J., Gritsch, S., Wiegand, G. & Rädler, J. O. Wetting of phospholipid membranes on hydrophilic surfaces—concepts towards self-healing membranes. *Eur. Phys. J. B* **10**, 335–344 (1999).
97. Ohlsson, G. et al. A miniaturized flow reaction chamber for use in combination with QCM-D sensing. *Microfluid. Nanofluid.* **9**, 705–716 (2010).
98. Sauerbrey, G. Use of quartz vibration for weighing thin films on a microbalance. *J. Phys.* **155**, 206–222 (1959).
99. Dodd, C. E. et al. Native *E. coli* inner membrane incorporation in solid-supported lipid bilayer membranes. *Biointerphases* **3**, FA59–FA67 (2008).
100. Hsia, C.-Y., Chen, L., Singh, R. R., DeLisa, M. P. & Daniel, S. A molecularly complete planar bacterial outer membrane platform. *Scientific Rep.* **6**, 32715 (2016).
101. Liu, H.-Y. et al. Supported planar mammalian membranes as models of in vivo cell surface architectures. *ACS Appl. Mater. Interfaces* **9**, 35526–35538 (2017).
102. Pace, H. et al. Preserved transmembrane protein mobility in polymer-supported lipid bilayers derived from cell membranes. *Anal. Chem.* **87**, 9194–9203 (2015).
103. Pace, H. P. et al. Structure and composition of native membrane derived polymer-supported lipid bilayers. *Anal. Chem.* **90**, 13065–13072 (2018).
104. Peerboom, N. et al. Cell membrane derived platform to study virus binding kinetics and diffusion with single particle sensitivity. *ACS Infect. Dis.* **4**, 944–953 (2018).
105. Richards, M. J. et al. Membrane protein mobility and orientation preserved in supported bilayers created directly from cell plasma membrane blebs. *Langmuir* **32**, 2963–2974 (2016).
106. Simonsson, L., Gunnarsson, A., Wallin, P., Jönsson, P. & Höök, F. Continuous lipid bilayers derived from cell membranes for spatial molecular manipulation. *J. Am. Chem. Soc.* **133**, 14027–14032 (2011).
107. Griebenow, K. & Klibanov, A. M. On protein denaturation in aqueous–organic mixtures but not in pure organic solvents. *J. Am. Chem. Soc.* **118**, 11695–11700 (1996).

Acknowledgements

This work was supported by the National Research Foundation of Singapore through a Proof-of-Concept grant (NRF2015NRF-POC0001-19) to N.-J.C. Additional support was provided by the Creative Materials Discovery Program through the National Research Foundation of Korea, funded by the Ministry of Science, ICT and Future Planning (NRF-2016M3D1A1024098) to N.-J.C.

Author contributions

A.R.F., J.A.J., and N.-J.C. designed the study. A.R.F., J.A.J., and N.-J.C. wrote the initial draft of the manuscript. B.K.Y., T.N.S., S.P., H.C., and J.H.P. contributed to protocol development. A.R.F., B.K.Y., T.N.S., S.P., H.C. J.H.P., and J.A.J. interpreted the results. N.-J.C. obtained funding. All authors reviewed, edited, and approved the paper.

Competing interests

The authors declare no competing interests.

Additional information

Supplementary information is available for this paper at https://doi.org/10.1038/s41596-019-0174-2.

Correspondence and requests for materials should be addressed to J.A.J. or N-J.C.

Journal peer review information: *Nature Protocols* thanks Ling Chao and other anonymous reviewer(s) for their contribution to the peer review of this work.

Received: 17 December 2018; Accepted: 2 April 2019;
Published online: 7 June 2019

Related links

Key references using this protocol

Tabaei, S. R., Jackman, J. A., Liedberg, B., Parikh, A. N. & Cho, N.-J. *J. Am. Chem. Soc.* **136**, 16962–16965 (2014): https://doi.org/10.1021/ja5082537
Tabaei, S. R., Choi, J.-H., Haw Zan, G., Zhdanov, V. P. & Cho, N.-J. *Langmuir* **30**, 10363–10373 (2014): https://doi.org/10.1021/la501534f
Tabaei, S. R., Jackman, J. A., Kim, S.-O., Zhdanov, V. P. & Cho, N.-J. *Langmuir* **31**, 3125–3134 (2015): https://doi.org/10.1021/la5048497
Vafaei, S., Tabaei, S. R., Biswas, K. H., Groves, J. T. & Cho, N. J. *Adv. Healthc. Mater.* **6**, 1700243 (2017): https://doi.org/10.1002/adhm.201700243

nature research

Corresponding author(s): Nam-Joon Cho & Joshua A. Jackman

Last updated by author(s): Mar 19, 2019

Reporting Summary

Nature Research wishes to improve the reproducibility of the work that we publish. This form provides structure for consistency and transparency in reporting. For further information on Nature Research policies, see Authors & Referees and the Editorial Policy Checklist.

Statistics

For all statistical analyses, confirm that the following items are present in the figure legend, table legend, main text, or Methods section.

n/a	Confirmed	
☐	☒	The exact sample size (*n*) for each experimental group/condition, given as a discrete number and unit of measurement
☒	☐	A statement on whether measurements were taken from distinct samples or whether the same sample was measured repeatedly
☒	☐	The statistical test(s) used AND whether they are one- or two-sided *Only common tests should be described solely by name; describe more complex techniques in the Methods section.*
☒	☐	A description of all covariates tested
☒	☐	A description of any assumptions or corrections, such as tests of normality and adjustment for multiple comparisons
☐	☒	A full description of the statistical parameters including central tendency (e.g. means) or other basic estimates (e.g. regression coefficient) AND variation (e.g. standard deviation) or associated estimates of uncertainty (e.g. confidence intervals)
☒	☐	For null hypothesis testing, the test statistic (e.g. *F*, *t*, *r*) with confidence intervals, effect sizes, degrees of freedom and *P* value noted *Give P values as exact values whenever suitable.*
☒	☐	For Bayesian analysis, information on the choice of priors and Markov chain Monte Carlo settings
☒	☐	For hierarchical and complex designs, identification of the appropriate level for tests and full reporting of outcomes
☒	☐	Estimates of effect sizes (e.g. Cohen's *d*, Pearson's *r*), indicating how they were calculated

Our web collection on statistics for biologists contains articles on many of the points above.

Software and code

Policy information about availability of computer code

Data collection	Biolin Scientific QSoft 401 2.6 for QCM-D data, Nikon NIS Elements AR 4.0 for fluorescence microscopy data
Data analysis	NIH ImageJ 1.51 for image analysis/processing, MathWorks MATLAB R2018b for FRAP analysis, Biolin Scientific QTools 3.1 for QCM-D data analysis/fitting, OriginLab OriginPro 8.5 for general data processing/plotting

For manuscripts utilizing custom algorithms or software that are central to the research but not yet described in published literature, software must be made available to editors/reviewers. We strongly encourage code deposition in a community repository (e.g. GitHub). See the Nature Research guidelines for submitting code & software for further information.

Data

Policy information about availability of data

All manuscripts must include a data availability statement. This statement should provide the following information, where applicable:

- Accession codes, unique identifiers, or web links for publicly available datasets
- A list of figures that have associated raw data
- A description of any restrictions on data availability

The datasets generated during and/or analysed during the current study are available from the corresponding authors on reasonable request.

Field-specific reporting

Please select the one below that is the best fit for your research. If you are not sure, read the appropriate sections before making your selection.

☒ Life sciences ☐ Behavioural & social sciences ☐ Ecological, evolutionary & environmental sciences

Life sciences study design

All studies must disclose on these points even when the disclosure is negative.

Sample size	Sample sizes were not pre-determined.
Data exclusions	No data was excluded.
Replication	All attempts at replication were successful.
Randomization	No randomization protocol was utilized.
Blinding	No blinding was involved.

Reporting for specific materials, systems and methods

We require information from authors about some types of materials, experimental systems and methods used in many studies. Here, indicate whether each material, system or method listed is relevant to your study. If you are not sure if a list item applies to your research, read the appropriate section before selecting a response.

Materials & experimental systems

n/a	Involved in the study
☐	☒ Antibodies
☒	☐ Eukaryotic cell lines
☒	☐ Palaeontology
☒	☐ Animals and other organisms
☒	☐ Human research participants
☒	☐ Clinical data

Methods

n/a	Involved in the study
☒	☐ ChIP-seq
☒	☐ Flow cytometry
☒	☐ MRI-based neuroimaging

Antibodies

Antibodies used	Anti-PtdIns(4)P IgM (anti-PI4P IgM; Echelon Biosciences, cat. no. Z-P004)
Validation	The antibody was validated by ensuring specificity through the use of mock controls, including supported lipid bilayers without PI(4)P (PC lipid only) or with PI alone (PC/PI composition) . Also, the manufacturer provided ELISA data that verified specific binding of the antibody to PI4P over PI and other PIP2 (PI3P and PI5P) lipids. Additional lipid blot data from the manufacturer further confirmed antibody binding specificity to PI4P over PI, PIP, other PIP2, and PIP3 lipids.